OPEN ACCESS
IOP Publishing
Plasma Physics and Controlled Fusion
Plasma Phys. Control. Fusion **66** (2024) 105016 (22pp)
https://doi.org/10.1088/1361-6587/ad6c7c

Linearised Fokker–Planck collision model for gyrokinetic simulations

A von Boetticher[1,*], F I Parra[2] and M Barnes[1]

[1] Rudolf Peierls Centre for Theoretical Physics, University of Oxford, Parks Road, Oxford OX1 3PU, United Kingdom
[2] Princeton Plasma Physics Laboratory, 100 Stellarator Road, Princeton, NJ, United States of America

E-mail: alexvboe@gmail.com

Received 25 February 2024, revised 1 May 2024
Accepted for publication 7 August 2024
Published 9 September 2024

Abstract

We introduce a gyrokinetic, linearised Fokker–Planck collision model that satisfies conservation laws and is accurate at arbitrary collisionalities. The differential test-particle component of the operator is exact; the integral field-particle component is approximated using a spherical harmonic and a modified Laguerre polynomial expansion developed by Hirshman and Sigmar (1976 *Phys. Fluids* **19** 1532). The numerical methods of the implementation in the δf-gyrokinetic code `stella` (Barnes *et al* 2019 *J. Comput. Phys.* **391** 365–80) are discussed, and conservation properties of the operator are demonstrated. The collision model is then benchmarked against the collision model of the gyrokinetic solver `GS2` in the limiting cases of a reduced test-particle collision operator and energy- and momentum-conserving operator. The accuracy of the full collision model is investigated by solving the parallel Spitzer-Härm problem for the transport coefficients. It is shown that retaining collisional energy flux and higher-order terms in the field-particle operator reduces errors in the transport coefficients from 10%–25% for a simple momentum- and energy-conserving model to under 1%.

Keywords: gyrokinetics, Fokker–Planck operator, stellarator, magnetic confinement fusion, turbulence

1. Introduction

The transport of heat and particles in stellarators is composed of a neoclassical and a turbulent contribution. In non-optimized stellarators, neoclassical transport can be significant and even exceed turbulent transport. In stellarators optimised for low neoclassical transport such as Wendelstein 7-X (W7-X), such transport is strongly reduced, and turbulence is relatively important: a comparison of measured heat fluxes in W7-X with calculated neoclassical fluxes suggests a turbulent contribution that is comparable to neoclassical transport levels [16]. Compared to tokamaks, relatively few numerical studies of turbulence have been performed for stellarators, and with some exceptions [e.g. 2, 15, 24], the gyrokinetic simulations in stellarators performed to date have mostly been collisionless. However, it is well known that collisions play a fundamental role in gyrokinetics as a dissipation mechanism, even in weakly collisional plasmas [1, 4] because the presence of a dissipation term is required for steady-state simulations of turbulence. Collisions can also be important in the relatively cool edge region of the plasma, as a detrapping mechanism for particles caught in magnetic wells [2] or for highly charged ion species, since the collision frequency scales with the fourth power of the species charge. The transport of impurity ions is especially relevant in magnetically confined plasmas because the accumulation of impurities in the plasma core leads to radiative energy loss via line radiation and Bremsstrahlung; in both cases, the power radiated increases with the impurity charge. The relatively high plasma density of future reactors may further increase the significance of collisions. These considerations motivate gyrokinetic simulations

* Author to whom any correspondence should be addressed.

of stellarator plasmas that account for the effect of particle collisions.

Collision models implemented in presently-available gyrokinetic codes typically simplify the Fokker–Planck operator by linearising and then replacing some of the integro-differential components of the linearised operator with simple approximations designed to ensure collisional conservation of momentum and energy. While this can be acceptable when collisional effects are relatively subdominant in the gyrokinetic equation, such a simplification inevitably becomes inaccurate when collisional effects are strong. Belli and Candy [7] have demonstrated the inaccuracy of commonly used approximations of the linearized Fokker–Planck operator at high collisionalities, using the drift-kinetic `NEO` code; Pan *et al* [23] have shown that the exact Fokker–Planck operator can yield significant corrections for growth rates of microinstabilties in tokamaks.

In this paper we present a new collision model for numerical simulations of stellarator turbulence, implemented in the gyrokinetic solver `stella` [5]. Accordingly, we work in the gyrokinetic framework. The strong magnetisation in fusion plasmas implies that the Larmor radius ρ_s is small compared to the scale length L of the macroscopic equilibrium:

$$\rho = \frac{v_{th}}{\Omega} \ll L, \tag{1}$$

where $\Omega = qB_0/(mc)$ is the cyclotron frequency, q denotes the particle charge, B_0 the magnetic field strength, m the particle mass, c is the speed of light in vacuum, and $v_{th} = \sqrt{2T_0/m}$ is the thermal velocity for an equilibrium temperature T_0. Equation (1) defines the small parameter $\epsilon := \rho/L \ll 1$. In the gyrokinetic framework [see 14], the plasma distribution function can be written to first order in ϵ as

$$f(\boldsymbol{r}, v_\parallel, v_\perp, \varphi) = F_0 \underbrace{- \frac{q\phi}{T_0} F_0 + h(\boldsymbol{R}, v_\parallel, v_\perp)}_{:=\delta f} + O(\epsilon^2), \tag{2}$$

where $F_0(\boldsymbol{r}, v_\parallel, v_\perp)$ denotes the equilibrium Maxwellian distribution, $\boldsymbol{r}$ is the particle position, $v_\parallel$ and $v_\perp$ denote the velocity components that are parallel and perpendicular to the magnetic field, respectively. The second term on the right-hand side describes the Boltzmann response of the particles to the electrostatic potential, $\phi(\boldsymbol{r})$. The guiding center distribution function $h(\boldsymbol{R}, v_\parallel, v_\perp) := \delta f + q\phi F_0/T_0$ represents the non-Boltzmann component of the first order perturbation δf_1 and is independent of the gyroangle when expressed in coordinates of the particle guiding center $\boldsymbol{R} := \boldsymbol{r} - \boldsymbol{\rho}$, where $\boldsymbol{\rho} = \hat{\boldsymbol{b}} \times \boldsymbol{v}/\Omega$ denotes the gyroradius. The electrostatic gyrokinetic equation for the guiding center distribution function is given by [see 14]

$$\frac{\partial h}{\partial t} + \left(v_\parallel \hat{\boldsymbol{b}} + \boldsymbol{v_D} + \langle \boldsymbol{v_E} \rangle_{\boldsymbol{R}}\right) \cdot \nabla h - \frac{\mu}{m} \hat{\boldsymbol{b}} \cdot \nabla \boldsymbol{B} \frac{\partial h}{\partial v_\parallel} + \left(\langle \boldsymbol{v_E} \rangle_{\boldsymbol{R}} \cdot \nabla - \frac{q}{T_0} \frac{\partial \langle \phi \rangle}{\partial t}\right) F_0 = \langle C[h] \rangle_{\boldsymbol{R}}. \tag{3}$$

where $\langle \cdot \rangle = 1/(2\pi) \int_0^{2\pi} \mathrm{d}\varphi$ denotes the gyroaverage, performed at fixed guiding-center $\boldsymbol{R}$, the unit vector of the magnetic field is denoted by $\boldsymbol{b} := \boldsymbol{B}/B_0$, and $\boldsymbol{v}_D$ and $\boldsymbol{v}_E$ are the magnetic and $\boldsymbol{E} \times \boldsymbol{B}$-drift velocities, respectively. The term $\langle C[h] \rangle_{\boldsymbol{R}}$ describes the influence of particle collisions on h. The gyrokinetic equation describes the dynamics of a distribution function of charged rings, obtained by averaging over the fast Larmor gyration of the particles around the magnetic field lines. In the following sections, we shall focus on the collision term in equation (3). The paper is organised as follows: we begin by introducing the linearised Fokker–Planck collision operator and its test- and field-particle components. The differential test-particle component is briefly described and converted into the velocity-space coordinate system employed by `stella`. We then introduce a systematic approximation of the integral field-particle component that is based on a series expansion designed to retain pertinent properties of the exact operator when the expansion is truncated for practical implementation. The full collision model is then converted into gyrokinetic form and the implementation in `stella` is discussed. We conclude by performing various numerical tests and demonstrate the accuracy of the collision model by solving the classical Spitzer problem for the transport coefficients.

2. Linearized collision operator

The effect of pair-wise small-angle Coulomb collisions between distribution functions of two species f_a and f_b is described by the Landau–Fokker–Planck operator [see 12, 19]

$$C_{ab}[f_a, f_b] = \frac{\partial}{\partial v_k} \left[A_k^{ab} f_a + \frac{\partial}{\partial v_l} \left(D_{kl}^{ab} f_a \right) \right], \tag{4}$$

where the Einstein summation convention is used and the tensors A_k^{ab} and D_{kl}^{ab} are given by

$$A_k^{ab} := L^{ab} [1 + m_a/m_b] \frac{\partial}{\partial v_k} \underbrace{\int \frac{f_b(\boldsymbol{v}')}{u} \, \mathrm{d}^3 v'}_{=:\, \phi_b(\boldsymbol{v})}$$
$$D_{kl}^{ab} := -L^{ab} \frac{\partial^2}{\partial v_k \partial v_l} \underbrace{\int u f_b(\boldsymbol{v}') \, \mathrm{d}^3 v'}_{=:\, \psi_b(\boldsymbol{v})}, \tag{5}$$

with $u := |\boldsymbol{v} - \boldsymbol{v}'|$ and $L^{ab} := (e_a e_b/m_a \epsilon_0)^2 \ln \Lambda$, where $\ln \Lambda$ is the Coulomb logarithm. We have also defined the Rosenbluth potentials $\phi_b(\boldsymbol{v})$ and $\psi_b(\boldsymbol{v})$. The Landau–Fokker–Planck operator exhibits several important physical properties of collisions: By taking the relevant moments of (4) it can be shown that the particle number, momentum, and energy are conserved. The collision operator vanishes for a Maxwellian distribution function. The operator is also self-adjoint and as a result can be shown to satisfy an H-theorem, ensuring that the total entropy of the plasma cannot decrease under collisions [see 12].

The amplitude of plasma fluctuations in fusion reactor cores is typically much smaller than the equilibrium, so that

the distribution function can be decomposed as introduced in equation (2), into an equilibrium and a fluctuating component viz. $f = F_0 + \delta f$, with $\delta f/F_0 = \epsilon \ll 1$. The collision operator can then be written as

$$C^{ab}\left[f_a,f_b\right] = C^{ab}\left[F_{0a},F_{0b}\right] + C^{ab}_{\text{test}}\left[\delta f_a,F_{0b}\right] + C^{ab}_{\text{field}}\left[F_{0a},\delta f_b\right] + O\left(\epsilon^2\right). \tag{6}$$

The zeroth-order term describes the collisional temperature equilibration between species and vanishes for $T_a = T_b$. For $T_a \neq T_b$ the term enters into the transport equations that describe the evolution of the equilibrium; subtracting the average of the transport equation over space-time scales that are long compared to the turbulent length scale, but short compared to the variations of the equilibrium eliminates the zeroth-order term from the gyrokinetic equation. The first, first-order, 'test-particle' term describes collisions of particles in the perturbed distribution function of species a, with the Maxwellian background of species b; the second, 'field-particle' term describes collisions of the background particles of species a with the perturbed particles of species b. The two operators have manifestly different structures; their derivations, conversions to gyrokinetic form, and numerical implementations are described separately in what follows.

2.1. Test-particle operator

The Rosenbluth potentials $\phi_b(\boldsymbol{v})$ and $\psi_b(\boldsymbol{v})$ simplify for Maxwellian distribution functions, as they are isotropic in velocity space. The test-particle operator can then be written as

$$C^{ab}_{\text{test}}\left[\delta f_a,F_{0b}\right] = L^{ab}\frac{\partial}{\partial v_k}\left[\frac{v_k}{v}\phi'_{0b}\delta f_a - \left(\frac{\left[v^2\delta_{kl}-v_kv_l\right]}{v^3}\psi'_{0b} + \frac{v_kv_l}{v^2}\psi''_{0b}\right)\frac{\partial \delta f_a}{\partial v_l}\right], \tag{7}$$

where primes denote derivatives with respect to the velocity magnitude, v, and the subscript '$0b$' indicates Rosenbluth potentials of Maxwellian distribution functions for species b. In the commonly used $(v,\ \xi := \cos\theta,\ \varphi)$-velocity space coordinate system, where $\theta = \arccos(v_\parallel/v)$ denotes the pitch angle, φ is the gyroangle and v the particle speed, the test-particle operator takes the familiar form

$$C^{ab}_{\text{test}}\left[\delta f_a,F_{0b}\right] = \frac{1}{2}\nu^{ab}_D\frac{\partial}{\partial\xi}\left(1-\xi^2\right)\frac{\partial\delta f_a}{\partial\xi} + \frac{1}{2}\nu^{ab}_D\frac{1}{1-\xi^2}\frac{\partial^2\delta f_a}{\partial\varphi^2} + \frac{1}{v^2}\frac{\partial}{\partial v}\left[\frac{1}{2}\nu^{ab}_\parallel v^4F_{0a}\frac{\partial}{\partial v}\frac{\delta f_a}{F_{0a}}\right], \tag{8}$$

and so separates into three differential terms in the three coordinates, describing diffusion in pitch-angle, gyro-angle and energy, respectively. We have introduced the velocity-dependent collision frequencies [12]

$$\nu^{ab}_D := \nu^{ab}\frac{\text{erf}\left(x_b\right)-G\left(x_b\right)}{x_a^3}, \tag{9}$$

$$\nu^{ab}_S := \nu^{ab}\frac{4G\left(x_b\right)}{x_a} \tag{10}$$

$$\nu^{ab}_\parallel := \frac{1}{2}\frac{\nu^{ab}_S}{x_a^2} \tag{11}$$

where $x_s = v/v_{th,s}$ with species index $s \in \{a,b\}$ and the Chandrasekhar function is given by $G(x) := [\text{erf}(x) - x\text{erf}'(x)]/2x^2$. The basic Spitzer collision frequency ν^{ab} is given by

$$\nu^{ab} = \frac{n_be_a^2e_b^2\ln\Lambda}{4\pi\,\epsilon_0^2m_a^2v_{th,a}^3}. \tag{12}$$

In the $(v_\parallel,\mu,\varphi)$-coordinate system employed by `stella`, where $\mu := mv_\perp^2/2B_0$ denotes the magnetic moment, the collision operator can be written as

$$C^{ab}_{\text{test}}\left[\delta f_a,F_{0b}\right] = \frac{\partial}{\partial v_\parallel}\left[\gamma^{ab}_{v_\parallel}F_{0a}\frac{\partial}{\partial v_\parallel}\frac{\delta f_a}{F_{0a}} + v_\parallel\mu\nu^{ab}_xF_{0a}\frac{\partial}{\partial\mu}\frac{\delta f_a}{F_{0a}}\right] + \frac{\partial}{\partial\mu}\left[\gamma^{ab}_\mu F_{0a}\frac{\partial}{\partial\mu}\frac{\delta f_a}{F_{0a}} + v_\parallel\mu\nu^{ab}_xF_{0a}\frac{\partial}{\partial v_\parallel}\frac{\delta f_a}{F_{0a}}\right] + \frac{\nu^{ab}_D}{2}\left[1+\frac{m_av_\parallel^2}{2B_0\mu}\right]\frac{\partial^2\delta f_a}{\partial\varphi^2}, \tag{13}$$

where $\nu^{ab}_x := \nu^{ab}_\parallel - \nu^{ab}_D$. Arranging the operator such that derivatives act on $\delta f_a/F_{0a}$ yields a more compact expression and, as we will see, has advantages for the numerical implementation of the operator. For convenience we have also defined the functions

$$\gamma^{ab}_\mu := 2\left[\nu^{ab}_\parallel\mu^2 + \nu^{ab}_D\frac{m_av_\parallel^2}{2B_0}\mu\right] \tag{14}$$

and

$$\gamma^{ab}_{v_\parallel} := \frac{1}{2}\left[\nu^{ab}_\parallel v_\parallel^2 + \nu^{ab}_D\frac{2B_0\mu}{m_a}\right]. \tag{15}$$

Equation (13) shows that switching from (ξ,v)-coordinates to a system that uses the parallel velocity and magnetic moment introduces mixed-differential terms in the collision operator. Terms occurring in the $v_\parallel$-derivative operator vanish at $v_\parallel \to \pm\infty$; terms in the μ-derivative operator vanish for $\mu \to 0$ and $\mu \to \infty$. These asymptotics will be relevant for the numerical implementation of the collision operator; relevant terms are shown in figures 1 and 2.

2.2. Field-particle operator

It can be shown that the test particle operator (equation (13)) alone does not conserve momentum and energy [see 12], as is desirable for a physical collision model. To ensure that these quantities are conserved requires that the field particle operator be included in the collision model. After linearisation

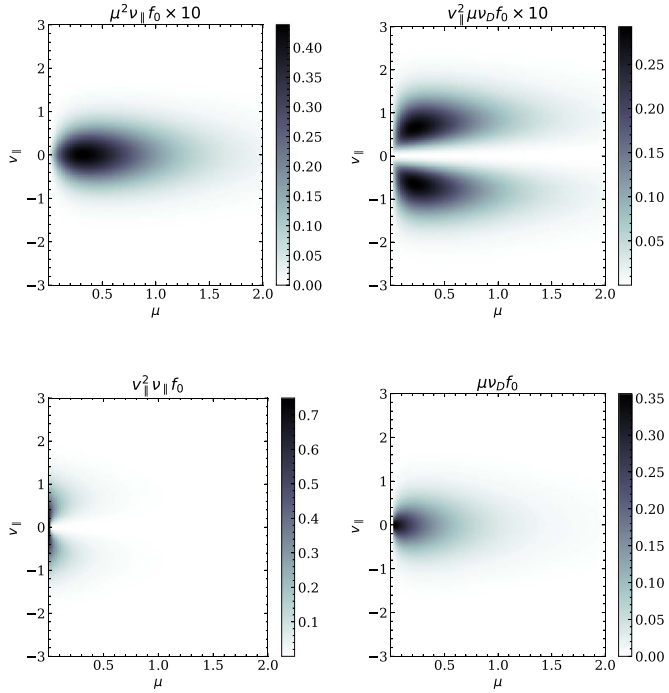

Figure 1. Collision frequency terms occurring in the test particle operator (13), for like-species collisions. Top row: terms occurring in the μ-differential term, vanishing for $\mu \to 0$ and $\mu \to \infty$. Bottom row: terms in the $v_\parallel$-derivative term, vanishing for $v_\parallel \to \pm\infty$.

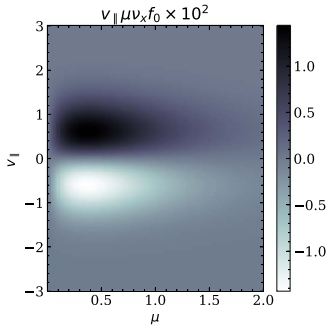

Figure 2. Collision frequency term occurring in the mixed-derivative terms of the test particle operator (13), for like-species collisions. The term vanishes for $\mu \to 0$ and $\mu \to \infty$, and for $v_\parallel \to \pm\infty$.

of the collision operator, the field particle component can be written as

$$C^{ab}_{\text{field}}\left[F_{0a}, \delta f_b\right] = \frac{\partial}{\partial v_k}\left[L^{ab}\left(1+\frac{m_a}{m_b}\right)\frac{\partial \phi_{b1}}{\partial v_k}F_{0a} + \frac{\partial}{\partial v_l}\left(-L^{ab}\frac{\partial^2 \psi_{b1}}{\partial v_k \partial v_l}F_{0a}\right)\right], \tag{16}$$

where the Rosenbluth potentials are now integral functionals of the perturbed distribution δf_b. Instead of dealing with the full field particle operator of equation (16), gyrokinetic codes commonly use a simpler ad hoc operator designed only to offset the momentum and energy produced by the test particle component to ensure overall momentum and energy conservation [1, 4, 7, 25]. In weakly collisional regimes this can be acceptable, but inevitably becomes inaccurate for high collisionalities. We therefore seek a method that approximates equation (16), is amenable to implementation in gyrokinetic codes, and, ideally, offers some flexibility to control the trade-off between accuracy and computational cost, as may be sensible for different physical regimes.

A natural starting point is to look for an expansion of equation (16). In the following section we review the approach of Hirshman and Sigmar [13], that has several properties that are desirable for a practical collision model. We describe this model, convert it into a form compatible with the gyrokinetic equation, and then turn to the implementation.

2.2.1. Expansion in spherical harmonics. The spherical symmetry of collisions in a plasma motivates an expansion of the distribution function in spherical harmonics; indeed we will see that these are eigenfunctions of the collision operator [12, 13, see]. We expand the perturbed piece of the distribution function

$$\delta f_b\left(v\right) = \sum_{l=0}^{\infty}\sum_{m=-l}^{+l} f_b^{(lm)}\left(v\right) Y_{lm}\left(\theta,\varphi\right), \tag{17}$$

where the expansion coefficients are given by

$$f_b^{(lm)}\left(v\right) = \iint \delta f_b\left(v,\theta,\varphi\right) Y^*_{lm}\left(\theta,\varphi\right)\, \sin\theta \mathrm{d}\theta \mathrm{d}\varphi. \tag{18}$$

Here $Y_{lm}(\theta,\varphi)$ denote the spherical harmonics of degree l and order m, and the superscript * denotes complex conjugation. The field particle operator then becomes

$$C^{ab}_{\text{field}}\left[F_{0a}, \delta f_b\right] = \sum_{l=0}^{\infty}\sum_{m=-l}^{+l} Y_{lm}\left(\theta,\varphi\right) C^{ab}_v\left[f_b^{(lm)}\left(v\right)\right], \tag{19}$$

where $C^{ab}_v[f_b^{(lm)}(v)]$ is an isotropic operator that will be addressed shortly. The expansion in spherical harmonics has a useful implication for the velocity moments of the collision operator: the kth velocity moment is given by

$$\begin{aligned}\int \mathbf{v}^k C^{ab}_{\text{field}}\left[F_{0a}, \delta f_b\right]\, \mathrm{d}\mathbf{v} &= \sum_{l=0}^{\infty}\sum_{m=-l}^{+l}\iiint \hat{\mathbf{v}}^k Y_{lm}\left(\theta,\varphi\right) \\ &\cdot v^k C^{ab}_v\left[f_b^{(lm)}\left(v\right)\right] v^2 \mathrm{d}v \sin\theta \mathrm{d}\theta \mathrm{d}\varphi \\ &= \sum_{l=0}^{k}\sum_{m=-l}^{+l}\int \boldsymbol{\nu}^k Y_{lm}\left(\theta,\varphi\right) C^{ab}_v\left[f_b^{(lm)}\left(v\right)\right] \mathrm{d}\mathbf{v},\end{aligned} \tag{20}$$

where the moment $\mathbf{v}^k$ is defined in terms of the tensor product and $\hat{\boldsymbol{\nu}}$ denotes the velocity unit vector. In equation (20) we used that $\hat{\boldsymbol{\nu}}^k$ can be expressed as a series of spherical harmonics up to degree k and the orthogonality of the spherical harmonics.

Retaining terms up to $l=k$ in the spherical harmonic expansion is therefore sufficient to exactly represent the first $k+1$ moments of the field particle operator. For notational clarity, we suppress the m-indices of the spherical harmonic expansion in what follows.

2.2.2. Hirshman-Sigmar expansion. The isotropic operator $C_v^{ab}[f_b^{(l)}(v)]$ remains complicated. A common method in transport calculations is to expand the coefficients $f_b^{(l)}(v)$ around a Maxwellian in generalized Laguerre polynomials $v^l L_j^{(l+\frac{1}{2})}(v^2)$ [13]

$$f_b^{(l)}(v) = \sum_{j=0}^{\infty} \frac{2}{v_{th,b}^{2l}} F_j^{(l)} v^l L_j^{\left(l+\frac{1}{2}\right)}\left(x_b^2\right) F_{0b}\left(x_b^2\right), \tag{21}$$

where $x_b := v/v_{th,b}$ and the expansion coefficients, $F_j^{(l)}$, are given by

$$F_j^{(l)} = \frac{\pi^{3/2} j!}{\left(j+l+\frac{1}{2}\right)!} \int_0^{\infty} v^l L_j^{\left(l+\frac{1}{2}\right)}\left(x_b^2\right) f_b^{(l)}(v)\, v^2 \mathrm{d}v. \tag{22}$$

The isotropic component of the field particle operator can then be written as

$$C_v^{ab}\left[f_b^{(l)}(v)\right] = \frac{2}{v_{th,b}^l} \sum_{j=0}^{\infty} F_j^{(l)} C_v^{ab}\left[x_b^l L_j^{\left(l+\frac{1}{2}\right)}\left(x_b^2\right) F_{0b}\left(x_b^2\right)\right]. \tag{23}$$

An approximation to the field particle operator can be obtained in this way by truncating this series at a finite $j_{\max} = N$. By invoking the orthogonality relation of the Laguerre polynomials in equation (22) for $f_b^{(l)}(v) = F_{0b}(v)$ it can be shown that the truncated series vanishes on a Maxwellian distribution function, as required for a physical model collision operator. However, the approximate operator given by the truncated expansion is not self-adjoint and fails to recover the velocity moments of the exact field particle operator—for that to hold requires the expansion coefficients to be moments of the collision operator [13].

To address these shortcomings, Hirshman and Sigmar [13] developed a modified expansion, that if truncated, guarantees the preservation of a subset of moments and retains the self-adjointness of the exact field particle operator. To develop the Hirshman-Sigmar expansion we proceed as follows, starting from the Laguerre expansion given by (23), with the set of basis functions

$$\left\{ C_v^{ab}\left[x_b^l L_j^{\left(l+\frac{1}{2}\right)}\left(x_b^2\right) F_{0b}\left(x_b^2\right)\right] \right\}_j. \tag{24}$$

A new set of basis functions, $\left\{\Delta_j^{ab}\right\}$ can then be constructed by using the Gram-Schmidt process, given by

$$\Delta_0^{ab}\left[x_b^l L_0^{\left(l+\frac{1}{2}\right)}\left(x_b^2\right) F_{0b}\left(x_b^2\right)\right] = C_v^{ab}\left[x_b^l L_0^{\left(l+\frac{1}{2}\right)}\left(x_b^2\right) F_{0b}\left(x_b^2\right)\right]$$

and

$$\Delta_{j+1}^{ab}\left[x_b^l L_{j+1}^{\left(l+\frac{1}{2}\right)}\left(x_b^2\right) F_{0b}\left(x_b^2\right)\right] = C_v^{ab}\left[x_b^l L_{j+1}^{\left(l+\frac{1}{2}\right)}\left(x_b^2\right) F_{0b}\left(x_b^2\right)\right] - \sum_{k=0}^{j} \psi_k^{ab} \Delta_k^{ab}\left[x_b^l L_k^{\left(l+\frac{1}{2}\right)} F_{0b}\left(x_b^2\right)\right]. \tag{25}$$

where the ψ_k^{ab} denote projection coefficients. Using the linearity of the Δ_j^{ab} and basis properties of the $x_b^l L_0^{(l+\frac{1}{2})}(x_b^2) F_{0b}(x_b^2)$, equation (25) defines the operators $\Delta_0^{ab}[f] = C_v^{ab}[f]$ and

$$\Delta_{j+1}^{ab}[f] = C_v^{ab}[f] - \sum_{k=0}^{j} \psi_k^{ab}[f] \Delta_k^{ab}\left[x_b^l L_k^{\left(l+\frac{1}{2}\right)} F_{0b}\left(x_b^2\right)\right] \tag{26}$$

acting on a general function f. Rearranging (26), the isotropic component of the exact collision operator, acting on the spherical harmonic expansion coefficients $f_b^{(l)}$, can then be written as

$$C_v^{ab}\left[f_b^{(l)}\right] = \sum_{k=0}^{j} \psi_k^{ab}\left[f_b^{(l)}\right] \Delta_k^{ab}\left[x_b^l L_k^{\left(l+\frac{1}{2}\right)} F_{0b}\left(x_b^2\right)\right] + \Delta_{j+1}^{ab}\left[f_b^{(l)}\right]. \tag{27}$$

An approximation of the collision operator can thus be obtained by summing to some $j_{\max} = N$ and neglecting Δ_{N+1}^{ab} in (27). Instead of choosing the projection coefficients ψ_k^{ab} as in the classical Gram-Schmidt process, so that the new basis functions form an orthogonal set, we instead determine the ψ_k to ensure that the truncated expansion meets the physical requirements of self-adjointness and moment preservation.

To ensure that the truncated expansion satisfies the self-adjointness condition of the collision operator [see 12] requires

$$\sum_{k=0}^{N} \psi_k^{ab}[g F_{0b}] \int h \Delta_k^{ab}\left[x_b^l L_k^{\left(l+\frac{1}{2}\right)} F_{0b}\left(x_b^2\right)\right] v^2 \mathrm{d}v = \sum_{k=0}^{N} \psi_k[h F_{0b}] \int g \Delta_k^{ab}\left[x_b^l L_k^{\left(l+\frac{1}{2}\right)} F_{0b}\left(x_b^2\right)\right] v^2 \mathrm{d}v \tag{28}$$

for any two functions $h(v)$ and $g(v)$. To ensure this holds we can set

$$\psi_k^{ab}[f] = \frac{1}{N_k^{(l)}} \int \frac{f}{F_{0a}} \Delta_k^{ab}\left[x_b^l L_k^{\left(l+\frac{1}{2}\right)} F_{0b}\left(x_b^2\right)\right] v^2 \mathrm{d}v, \tag{29}$$

where $N_k^{(l)}$ denotes a constant. The operators $\Delta_j^{ab}[f]$ defined by (25) are self-adjoint. To see this, we can write the Gram-Schmidt step (25) for $\Delta_j^{ab}[f]$ and subtract from the expression for $\Delta_{j+1}^{ab}[f]$ to obtain

$$\Delta_{j+1}^{ab}[f] = \Delta_j^{ab}[f] - \psi_j^{ab}[f]\,\Delta_j^{ab}\left[x_b^l L_j^{(l+\frac{1}{2})}\left(x_b^2\right) F_{0b}\left(x_b^2\right)\right]. \quad (30)$$

Since $\Delta_0^{ab}[f] = C_v^{ab}[f]$ is a self-adjoint operator, it is straightforward to verify from (30) that by induction all $\Delta_j^{ab}[f]$ are self-adjoint operators.

We now consider the velocity moments of the collision operator. Taking the nth velocity moment of (27), we see that for the truncated expansion to recover the moment of the exact field particle operator:

$$\int v^n C_v^{ab}\left[f_b^{(l)}\right] v^2 \mathrm{d}v = \int v^n \sum_{k=0}^{N} \psi_k^{ab}\left[f_b^{(l)}\right] \times \Delta_k^{ab}\left[x_b^l L_k^{(l+\frac{1}{2})} F_{0b}\left(x_b^2\right)\right] v^2 \mathrm{d}v, \quad (31)$$

requires that

$$\int v^n \Delta_{N+1}^{ab}\left[f_b^l\right] v^2 \mathrm{d}v = 0. \quad (32)$$

Since the monomial v^n can be exactly expressed using a finite linear combination of the $v^l L_j^{(l+\frac{1}{2})}(v^2)$ we can ensure that $\Delta_{N+1}^{ab}\left[f_b^l\right]$ is orthogonal to a subset of the $v^l L_j^{(l+\frac{1}{2})}(v^2)$ for moment preservation. Multiplying (30) by $v^l L_j^{(l+\frac{1}{2})}(v^2)$, integrating, and using the self-adjointness of the Δ_j^{ab}, it follows that by setting the N_k^l to

$$N_k^{(l)} := \int_0^\infty x_a^l L_j^{(l+\frac{1}{2})}\left(x_a^2\right) \Delta_j^{ab}\left[x_b^l L_j^{(l+\frac{1}{2})}\left(x_b^2\right) F_{0b}\right] v^2 \mathrm{d}v, \quad (33)$$

we can ensure that $\Delta_{N+1}\left[f_b^l\right]$ is orthogonal to the velocity moment $v^l L_N^{(l+\frac{1}{2})}(v^2)$. It is shown by induction in appendix A that then

$$\int v^l L_j^{(l+\frac{1}{2})}\left(v^2\right) \Delta_{N+1}^{ab}\left[f_b^l\right] v^2 \mathrm{d}v = 0 \quad \text{for all } j \leqslant N. \quad (34)$$

Truncating the expansion at $j_{\max} = N$ then exactly preserves a subset of the velocity moments of the field particle operator. A proof that the expansion of the isotropic component of the field particle operator converges to the exact operator [13] for $j_{\max} =: N \to \infty$ is reviewed in appendix A. With the truncated expansion defined by (27) and the expansion coefficients given by (29) and (33), we have therefore constructed an approximation of the isotropic component of the field particle operator that retains key physical properties of the exact field particle operator.

2.2.3. Calculation of Δ_0^{ab}. It remains to calculate the first element of the Hirshman-Sigmar expansion series, $\Delta_0^{ab}[x_b^l L_j^{(l+\frac{1}{2})}(x_b^2) F_{0b}] = C_v^{ab}[x_b^l L_j^{(l+\frac{1}{2})}(x_b^2) F_{0b}]$, where C_v^{ab} is the isotropic component of the field particle operator. The full calculation is provided in appendix B and yields

$$\begin{aligned}
&\Delta_0^{ab}\left[x_b^l L_j^{(l+1/2)}\left(x_b^2\right)\exp\left(-x_b^2\right)\right] \\
&= L^{ab}\mu_{ab}\exp\left(-x_a^2\right)\frac{1}{2l+1}\sum_{i=0}^{j} c_i^{(jl)}\left[(2l+1)\,x_b^{l+2i}\exp\left(-x_b^2\right)\right. \\
&\quad - x_b(1-\mu_{ab})\left(-\frac{l+1}{x_b^{l+2}}\gamma_{\frac{3}{2}+l+i}\left(x_b^2\right) + l x_b^{l-1}\Gamma_{1+i}\left(x_b^2\right)\right) \\
&\quad - \left(\frac{1}{x_b^{l+1}}\gamma_{\frac{3}{2}+l+i}\left(x_b^2\right) + x_b^l\Gamma_{1+i}\left(x_b^2\right)\right) \\
&\quad + \mu_{ab}x_b^2\frac{(l+1)(l+2)}{2l+3}\left(\frac{1}{x_b^{l+3}}\gamma_{\frac{5}{2}+l+i}\left(x_b^2\right) + x_b^l\Gamma_{1+i}\left(x_b^2\right)\right) \\
&\quad \left. - \mu_{ab}x_b^2\frac{l(l-1)}{2l-1}\left(\frac{1}{x_b^{l+1}}\gamma_{\frac{3}{2}+l+i}\left(x_b^2\right) + x_b^{l-2}\Gamma_{2+i}\left(x_b^2\right)\right)\right],
\end{aligned}$$

where $\gamma_i(x) := \gamma(i,x)$ and $\Gamma_i(x) := \Gamma(i,x)$ are the lower and upper incomplete Gamma functions, respectively, and the constant $c_i^{(jl)}$ is given by

$$c_k^{(jl)} = \frac{(-1)^k (l+j+1/2)!}{(j-k)!\,(l+k+1/2)!\,k!}. \quad (35)$$

For the purpose of the implementation of the collision operator, discussed in section 3, the incomplete gamma functions can be calculated recursively from the error function that is available in `FORTRAN`, using the standard recursion formulae,

$$\Gamma(s+1,x) = s\Gamma(s,x) + x^s\exp(-x) \quad (36)$$

and

$$\gamma(s+1,x) = s\gamma(s,x) - x^s\exp(-x), \quad (37)$$

for integer parameters s.

2.2.4. Combined expansion of the field particle operator. Combining the results of this section, the Hirshman-Sigmar field particle operator is given by

$$C_{\text{field}}^{ab}[F_{0a}, \delta f_b] = \sum_{l=0}^{\infty}\sum_{m=-l}^{+l} Y_{lm}(\theta,\varphi)\, C_v^{ab}\left[f_b^{(lm)}(v)\right], \quad (38)$$

where

$$f_b^{(lm)}(v) = \iint \delta f_b(v,\theta,\varphi)\, Y_{lm}^*(\theta,\varphi)\sin\theta \mathrm{d}\theta\mathrm{d}\varphi, \quad (39)$$

and

$$C_v^{ab}\left[f_b^{(lm)}\right] := \sum_{j=0}^{\infty}\psi_j^{ab,l}\left[f_b^{(lm)}\right]\Delta_j^{ab,l}. \quad (40)$$

where for compactness we have defined

$$\Delta_j^{ab,l} := \Delta_j^{ab}\left[x_b^l L_j^{(l+\frac{1}{2})}\left(x_b^2\right) F_{0b}\left(x_b^2\right)\right]. \quad (41)$$

Using the self-adjointness of the $\Delta_j^{ab}[\cdot]$, the expansion coefficients $\psi_j^{ab,l}$ are given by

$$\psi_j^{ab,l}\left[f_b^{(lm)}\right] = \frac{\int_0^\infty x_a^l L_j^{\left(l+\frac{1}{2}\right)}\left(x_a^2\right)\Delta_j^{ab}\left[f_b^{(lm)}\right]\, v^2 \mathrm{d}v}{\int_0^\infty x_a^l L_j^{\left(l+\frac{1}{2}\right)}\left(x_a^2\right)\Delta_j^{ab,l}\, v^2 \mathrm{d}v}. \quad (42)$$

2.3. Gyrokinetic form of the collision operator

To be compatible with the gyrokinetic equation (3), the collision operator is gyroaveraged. To facilitate this, the guiding center distribution function can be written spectrally in components of the guiding-center $\boldsymbol{R}$ that are perpendicular to the magnetic field

$$h = \sum_{\boldsymbol{k}_\perp} e^{i\boldsymbol{k}_\perp\cdot\boldsymbol{R}} h_{\boldsymbol{k}_\perp}\left(z, v_\parallel, \mu\right), \quad (43)$$

where z denotes the spatial coordinate along the field line, $\boldsymbol{R} = \boldsymbol{r} - \boldsymbol{\rho}$, and $\boldsymbol{r}$, $\boldsymbol{\rho} = \hat{\boldsymbol{b}} \times \boldsymbol{v}/\Omega$ and Ω denote the particle position, Larmor vector and cyclotron frequency, respectively. We shall suppress species indices for brevity in this section and reintroduce these later. The gyrokinetic collision operator then becomes [1]

$$\begin{aligned} C_{\mathrm{GK}}[h] &= \left\langle C\left[\sum_{\boldsymbol{k}_\perp} e^{i\boldsymbol{k}_\perp\cdot\boldsymbol{R}} h_{\boldsymbol{k}_\perp}\right]\right\rangle \\ &= \sum_{\boldsymbol{k}_\perp} \langle e^{i\boldsymbol{k}_\perp\cdot\boldsymbol{r}} C\left[e^{-i\boldsymbol{k}_\perp\cdot\boldsymbol{\rho}} h_{\boldsymbol{k}_\perp}\right]\rangle_{\boldsymbol{R}} \\ &= \sum_{\boldsymbol{k}_\perp} e^{i\boldsymbol{k}_\perp\cdot\boldsymbol{R}} \langle e^{i\boldsymbol{k}_\perp\cdot\boldsymbol{\rho}} C\left[e^{-i\boldsymbol{k}_\perp\cdot\boldsymbol{\rho}} h_{\boldsymbol{k}_\perp}\right]\rangle_{\boldsymbol{R}}, \end{aligned} \quad (44)$$

where $\langle h\rangle$ denotes the gyroaverage, performed at fixed guiding-center $\boldsymbol{R}$. The Fourier components of the gyrokinetic collision operator operator are then given by

$$C_{\mathrm{GK}}[h_{\boldsymbol{k}_\perp}] = \langle e^{i\boldsymbol{k}_\perp\cdot\boldsymbol{\rho}} C\left[e^{-i\boldsymbol{k}_\perp\cdot\boldsymbol{\rho}} h_{\boldsymbol{k}_\perp}\right]\rangle_{\boldsymbol{R}}. \quad (45)$$

2.3.1. Gyrokinetic test particle operator. The calculation of the Fourier components of the gyrokinetic test particle operator in $(v_\parallel, \mu)$-coordinates is performed in appendix C and yields

$$\begin{aligned} C_{\mathrm{GK,test}}\left[h_{\boldsymbol{k}_\perp}\right] &= \frac{\partial}{\partial v_\parallel}\left[\gamma_{v_\parallel} F_0 \frac{\partial}{\partial v_\parallel}\frac{h_{\boldsymbol{k}_\perp}}{F_0} + v_\parallel \mu \nu_x F_0 \frac{\partial}{\partial \mu}\frac{h_{\boldsymbol{k}_\perp}}{F_0}\right] \\ &+ \frac{\partial}{\partial \mu}\left[\gamma_\mu F_0 \frac{\partial}{\partial \mu}\frac{h_{\boldsymbol{k}_\perp}}{F_0} + v_\parallel \mu \nu_x F_0 \frac{\partial}{\partial v_\parallel}\frac{h_{\boldsymbol{k}_\perp}}{F_0}\right] \\ &- \frac{1}{2}\left(\nu_\parallel B_0 \mu/m + \nu_D\left[v_\parallel^2 + B_0\mu/m\right]\right)\frac{k_\perp^2\rho^2}{v_{th}^2} h_{\boldsymbol{k}_\perp}, \end{aligned} \quad (46)$$

where all velocity-space derivatives are understood to be performed at fixed guiding-center. The gyroaverage of the collision operator has eliminated the dependence on the gyroangle and introduced a spatial diffusive term that is proportional to the square of the thermal Larmor radius, $\rho = v_{th}/\Omega$, and the perpendicular wave number. In the following sections we drop spectral indices for clarity.

2.3.2. Gyrokinetic field particle operator. Turning to the field particle operator we perform the expansion in spherical harmonics

$$e^{-i\boldsymbol{k}_\perp\cdot\boldsymbol{\rho}} h_{\boldsymbol{k}_\perp} = \sum_{l=0}^{\infty}\sum_{m=-l}^{+l} Y_{lm}(\theta,\varphi)\, h_{\boldsymbol{k}_\perp}^{lm}(v), \quad (47)$$

with coefficients

$$\begin{aligned} h_{\boldsymbol{k}_\perp}^{lm}(v) &= \iint Y_{lm}^*(\theta,\varphi)\, e^{-i\boldsymbol{k}_\perp\cdot\boldsymbol{\rho}} h_{\boldsymbol{k}_\perp}\left(z, v_\parallel, \mu\right)\sin\theta \mathrm{d}\theta \mathrm{d}\varphi \\ &= c_{l,-m}\iint (-1)^m e^{-im\varphi + ikv_\perp \sin\varphi/\Omega}\mathrm{d}\varphi \\ &\quad \times P_{l,-m}(\cos\theta)\, h_{\boldsymbol{k}_\perp}\left(z, v_\parallel, \mu\right)\sin\theta \mathrm{d}\theta \\ &= 2\pi\, c_{l,-m}(-1)^m \int J_m\left(\frac{k_\perp v_\perp}{\Omega}\right) P_{l,-m}(\cos\theta) \\ &\quad \times h_{\boldsymbol{k}_\perp}\left(z, v_\parallel, \mu\right)\sin\theta \mathrm{d}\theta, \end{aligned} \quad (48)$$

where P_{lm} are the associated Legendre polynomials and we have used that $Y_{lm}(\theta,\varphi) = c_{lm}P_{lm}(\cos\theta)e^{im\varphi}$ with $c_{lm} = \sqrt{\frac{(2l+1)(l-m)!}{(4\pi)(l+m)!}}$; $\boldsymbol{k}_\perp\cdot\boldsymbol{\rho} = -kv_\perp\sin\varphi/\Omega$ and the Jacobi-Anger identity

$$J_n(x) = \frac{1}{2\pi}\int_0^{2\pi} e^{i(x\sin(\varphi) - n\varphi)}\,\mathrm{d}\varphi. \quad (49)$$

The gyrokinetic field particle operator is then given by

$$\begin{aligned} &C_{\mathrm{GK,field}}\left[h_{\boldsymbol{k}_\perp}\right] \\ &= \sum_{\boldsymbol{k}_\perp} e^{i\boldsymbol{k}_\perp\cdot\boldsymbol{R}}\left\langle e^{i\boldsymbol{k}_\perp\cdot\boldsymbol{\rho}} C_{\mathrm{field}}\left[\sum_{l=0}^{\infty}\sum_{m=-l}^{m=+l} Y_{lm}(\theta,\varphi)\, h_{\boldsymbol{k}_\perp}^{lm}(v)\right]\right\rangle_{\boldsymbol{R}} \\ &= \sum_{\boldsymbol{k}_\perp} e^{i\boldsymbol{k}_\perp\cdot\boldsymbol{R}}\sum_{l=0}^{\infty}\sum_{m=-l}^{m=+l}\left\langle e^{i\boldsymbol{k}_\perp\cdot\boldsymbol{\rho}} Y_{lm}(\theta,\varphi)\right\rangle_{\boldsymbol{R}} C_v^{ab}\left[h_{\boldsymbol{k}_\perp}^{lm}(v)\right], \end{aligned} \quad (50)$$

where in the last line we used that the spherical harmonics are eigenfunctions of the collision operator and C_v^{ab} is the isotropic component of the Hirshman-Sigmar field particle operator. With

$$\begin{aligned} \langle e^{i\boldsymbol{k}_\perp\cdot\boldsymbol{\rho}} Y_{lm}(\theta,\varphi)\rangle_{\boldsymbol{R}} &= \frac{1}{2\pi}\int_0^{2\pi} e^{i\boldsymbol{k}\cdot\boldsymbol{\rho}} Y_{lm}\,\mathrm{d}\varphi \\ &= c_{lm}P_{lm}(\cos\theta)\frac{1}{2\pi}\int_0^{2\pi} e^{-ikv_\perp\sin\varphi/\Omega + im\varphi}\,\mathrm{d}\varphi \end{aligned} \quad (51)$$

it follows that the kth Fourier component of the field particle operator is given by

$$\begin{aligned} &C_{\mathrm{GK,field}}\left[h_{\boldsymbol{k}_\perp}\right] \\ &= \sum_{l=0}^{\infty}\sum_{m=-l}^{+l} c_{lm}P_{lm}\left(\cos\theta\right)J_m\left(\frac{k_\perp v_\perp}{\Omega}\right)C_v\left[h^{lm}_{\boldsymbol{k}_\perp}\left(v\right)\right] \\ &= \sum_{l=0}^{\infty}\sum_{m=-l}^{+l}\sum_{j=0}^{\infty} c_{lm}P_{lm}\left(\cos\theta\right)J_m\left(\frac{k_\perp v_\perp}{\Omega}\right)\psi^l_j\left[h^{lm}_{\boldsymbol{k}_\perp}\left(v\right)\right] \\ &\quad\times\Delta^{(l)}_j\left(x^l L^{(l+1/2)}_j\left(x^2\right)F_0\right). \end{aligned} \tag{52}$$

where $x = v/v_{th}$ and species indices are suppressed. The coefficients ψ^l_j are given by

$$\begin{aligned} \psi^l_j\left[h^{lm}_{\boldsymbol{k}_\perp}\left(v\right)\right] = 2\pi\, c_{l,-m}\frac{(-1)^m}{N^l_j}\iint P_{l,-m}\left(\cos\theta\right)J_m\left(\frac{k_\perp v_\perp}{\Omega}\right) \\ \times h_{\boldsymbol{k}_\perp}\Delta^{(l)}_j\left[x^l L^{(l+1/2)}_j\left(x^2\right)F_0\left(x\right)\right]v^2\mathrm{d}v\sin\theta\mathrm{d}\theta, \end{aligned} \tag{53}$$

where N^l_j is the normalising factor $N^l_j := \iint x^l L^{(l+\frac{1}{2})}_j(x^2)\Delta^{(l)}_j[x^l L^{(l+1/2)}_j F_0(x)]v^2\mathrm{d}v\sin\theta\mathrm{d}\theta$. We have also used the self-adjointness of the operators $\Delta^{(l)}_j$ to obtain $\int x^l L^{(l+1/2)}_j(x^2)\Delta^{(l)}_j[h^{lm}_k]v^2\mathrm{d}v = \int\left(h^{lm}_k/F_0(x)\right)\Delta^{(l)}_j[x^l L^{(l+1/2)}_j(x^2)F_0(x)]v^2\mathrm{d}v$. To reduce the number of computations required in the numerical implementation, one may combine positive and negative m-indices in (52) by using $P_{l,-m} = (-1)^m(l-m)!/(l+m)!P_{lm}$ and $J_{-m} = (-1)^m J_m$ to obtain

$$\begin{aligned} &C_{\mathrm{GK,field}}\left[h_{\boldsymbol{k}_\perp}\right] \\ &= \sum_{l=1}^{\infty}\left(c_{l,0}P_{l,0}\left(\cos\theta\right)J_0\left(\frac{k_\perp v_\perp}{\Omega}\right)C_v\left[h^{l,0}_{\boldsymbol{k}_\perp}\left(v\right)\right]\right. \\ &\quad\left. + 2\sum_{m=1}^{+l} c_{lm}P_{lm}\left(\cos\theta\right)J_m\left(\frac{k_\perp v_\perp}{\Omega}\right)C_v\left[h^{lm}_{\boldsymbol{k}_\perp}\left(v\right)\right]\right). \end{aligned} \tag{54}$$

With this in hand, we turn to the numerical implementation of the collision model.

3. Numerical implementation

The code `stella` [5] solves the gyrokinetic equation in a general magnetic geometry, permitting simulations in the non-axisymmetric configurations of stellarators. The code advances the gyrokinetic equation in terms of the gyroaveraged distribution function $g := \langle\delta f\rangle = \langle h - q\phi F_0/T_0\rangle = h - q\langle\phi\rangle F_0/T_0$. The spatial coordinates perpendicular to the magnetic field, x and y, are treated spectrally by decomposing the distribution function into Fourier harmonics. This ensures periodicity in the perpendicular coordinates, an acceptable assumption because turbulence is statistically periodic over spatial scales that are short compared to the device size. The field-line parallel coordinate z is discretised on a uniform grid.

3.1. Velocity space discretisation

The gyrokinetic code `stella` employs $(v_\parallel,\mu)$-velocity space coordinates, where $v_\parallel$ is the velocity component parallel to the magnetic field, and $\mu = mv^2_\perp/2B_0$ denotes the magnetic moment. Velocity-space quantities are discretized on a uniformly spaced $v_\parallel$-grid and optionally on either a uniform or Gauss–Laguerre grid in the magnetic moment. The $v_\parallel$-grid is anti-symmetric around $v_\parallel = 0$, with $v_\parallel = 0$ not included in the grid. If a uniform μ-grid is employed, the smallest μ-value, μ_{min} is given by $\mu_{min} = \Delta_\mu/2$, where Δ_μ denotes the grid spacing in μ.

3.1.1. Uniform velocity grids. Derivatives in the test particle operator given by equation (46) are discretized using a three-point stencil for both velocity-space grids. In the $v_\parallel$ coordinate, at index i, and suppressing the μ-grid index j, the derivative is approximated by

$$\begin{aligned} \frac{\partial}{\partial v_\parallel}\left[G\left(v_\parallel\right)\frac{\partial h}{\partial v_\parallel}\right]_i \approx \frac{1}{\Delta_{v_\parallel}}\left[-G\left(v_{\parallel,i-\frac{1}{2}}\right)\left(\frac{\partial h}{\partial v_\parallel}\right)_{i-\frac{1}{2}}\right. \\ \left. + G\left(v_{\parallel,i+\frac{1}{2}}\right)\left(\frac{\partial h}{\partial v_\parallel}\right)_{i+\frac{1}{2}}\right], \end{aligned} \tag{55}$$

where for concision we have introduced $G(v_\parallel,\mu) = \gamma_{v_\parallel}F_0$, and assumed that h denotes the distribution function normalized by a Maxwellian F_0 as required in equation (46). Here $\left(\partial h/\partial v_\parallel\right)_{i-\frac{1}{2}} = (h_i - h_{i-1})/\Delta_{v_\parallel}$ and analogously for $\left(\partial h/\partial v_\parallel\right)_{i+\frac{1}{2}}$ where $\Delta_{v_\parallel}$ is the grid spacing in $v_\parallel$. For quantities evaluated at half-indices, $G_{i\pm\frac{1}{2}} = (G_i + G_{i\pm1})/2$. The discretisation scheme (55) is second order accurate in $\Delta_{v_\parallel}$ [4, see].

At the boundary indices $i = \{1, N\}$, we use $G_{N+1/2} = 0$ and $G_{1-1/2} = 0$, justified by the asymptotics described in section 2.1. It follows that

$$\sum_{i=1}^{N}\left[-G\left(x_{i-\frac{1}{2}}\right)\left(\frac{\partial h}{\partial x}\right)_{i-\frac{1}{2}} + G\left(x_{i+\frac{1}{2}}\right)\left(\frac{\partial h}{\partial x}\right)_{i+\frac{1}{2}}\right] = 0, \tag{56}$$

since the terms in the sum telescope vanish beyond boundary indices. Equation (56) implies that the numerical density integral of the terms discretised with the scheme (55) vanishes exactly—that is, independently of the velocity-space resolution—as is required for exact density conservation of the collision operator. If the weights of the integration scheme employed are uniform, the discretisation of the single-variable double derivative terms given by (55) also satisfies the numerical equivalents of integration by parts and the fundamental theorem of calculus. This can be readily verified by multiplying (55) by a test function, summing the index from $i = 1$ to $i = N$ and shifting summation indices where opportune. It follows from these properties that the discretisation scheme satisfies numerical self-adjointness. With the discretisation scheme (55) the coefficient of h_i is

$$\frac{1}{\Delta_i^2}\left(G_{i+1/2}-G_{i-1/2}\right), \tag{57}$$

and the coefficients of h_{i+1} and h_{i-1} are

$$\frac{1}{\Delta_i^2}G_{i+1/2} \tag{58}$$

and

$$-\frac{1}{\Delta_i^2}G_{i-1/2}, \tag{59}$$

respectively. The analogous scheme is employed for the term $\partial/\partial\mu(G(\mu)\partial h/\partial\mu)$.

The mixed derivative terms in equation (46) could be discretised using a standard centered difference. However, this scheme fails to guarantee density conservation and self-adjointness of the test particle operator. To retain this property the standard centered difference can be modified by using half-indices

$$\frac{\partial}{\partial v_\parallel}\left[G\frac{\partial h}{\partial\mu}\right]_{i,j}\approx\left[G_{i+\frac{1}{2},j}\left(\frac{\partial h}{\partial\mu}\right)_{i+\frac{1}{2},j}-G_{i-\frac{1}{2},j}\left(\frac{\partial h}{\partial\mu}\right)_{i-\frac{1}{2},j}\right]\Big/\Delta_{v_\parallel}, \tag{60}$$

where $h_{i\pm\frac{1}{2},j}=(h_{i,j}+h_{i\pm1,j})/2$. The inner derivative is approximated by

$$G_{i\pm\frac{1}{2},j}\left(\frac{\partial h}{\partial\mu}\right)_{i\pm\frac{1}{2},j}\approx\frac{1}{2}\left[G_{i\pm1/2,j+\frac{1}{2}}\frac{h_{i\pm1/2,j+1}-h_{i\pm\frac{1}{2},j}}{\Delta_\mu}+G_{i\pm\frac{1}{2},j-1/2}\frac{h_{i\pm\frac{1}{2},j}-h_{i\pm\frac{1}{2},j-1}}{\Delta_\mu}\right], \tag{61}$$

and G is again assumed to vanish at indices beyond the boundaries. Upon summation, density conservation follows immediately from the telescoping property of the series and boundary conditions. With this scheme the coefficient of $h_{i,j}$ is

$$\frac{1}{4\Delta_\mu\Delta_{v_\parallel}}\Big[\left(-G_{i+1/2,j+1/2}+G_{i+1/2,j-1/2}\right)-\left(-G_{i-1/2,j+1/2}+G_{i-1/2,j-1/2}\right)\Big], \tag{62}$$

and the coefficients of $h_{i,j\pm1}$ are

$$\frac{1}{4\Delta_\mu\Delta_{v_\parallel}}\left[\mp G_{i+1/2,j\pm1/2}\pm G_{i-1/2,j\pm1/2}\right]. \tag{63}$$

For $h_{i\pm1,j+1}$ one obtains

$$\pm\frac{1}{4\Delta_\mu\Delta_{v_\parallel}}\left(-G_{i\pm1/2,j+1/2}\right), \tag{64}$$

for $h_{i\pm1,j-1}$

$$\pm\frac{1}{4\Delta_\mu\Delta_{v_\parallel}}\left(G_{i\pm1/2,j-1/2}\right), \tag{65}$$

and for $h_{i\pm1,j}$ the coefficients are

$$\pm\frac{1}{4\Delta_\mu\Delta_{v_\parallel}}\left(-G_{i\pm1/2,j+1/2}+G_{i\pm1/2,j-1/2}\right). \tag{66}$$

The same scheme is used to discretise the term $\partial/\partial\mu(G\partial h/\partial v_\parallel)$.

3.1.2. Non-uniform Gauss–Laguerre μ-grid. `stella` can optionally use a μ-grid determined by Gauss–Laguerre quadrature. This grid has a non-uniform grid-spacing that decreases near the boundary $\mu=0$ for better resolution. On such a non-uniform grid, the two-point centered difference formula introduced previously is only first-order accurate. A second-order accurate scheme for the first derivative on a non-uniform grid is given by the three-point formula [see 18]

$$\left(\frac{\partial h}{\partial\mu}\right)_i\approx\frac{1}{\Delta_{i-1}+\Delta_i}\left[\frac{\Delta_{i-1}}{\Delta_i}h_{i+1}+\frac{\Delta_i^2-\Delta_{i-1}^2}{\Delta_{i-1}\Delta_i}h_i-\frac{\Delta_i}{\Delta_{i-1}}h_{i-1}\right]=\frac{1}{\Delta_{i-1}+\Delta_i}\left[\frac{\Delta_{i-1}}{\Delta_i}h'_{i+1/2}+\frac{\Delta_i}{\Delta_{i-1}}h'_{i-1/2}\right], \tag{67}$$

where $h'_{i+1/2}\approx(h_{i+1}-h_i)/\Delta_i$ with $\Delta_i=\mu_{i+1}-\mu_i$ and $h'_{i-1/2}\approx(h_i-h_{i-1})/\Delta_{i-1}$. Equation (67) resembles the weighted average of the centered differences at the half-indices $i+1/2$ and $i-1/2$. We obtain a three-point scheme for the term of the form $\partial/\partial\mu(G\partial h/\partial\mu)$ by identifying the outer indices in (67) with half-indices whence

$$\frac{\partial}{\partial\mu}\left[G(\mu)\frac{\partial h}{\partial\mu}\right]_i\approx\frac{2}{\Delta_{i-1}+\Delta_i}\left[\frac{\Delta_{i-1}}{\Delta_i}\left(Gh'\right)_{i+1/2}+\frac{\Delta_i^2-\Delta_{i-1}^2}{\Delta_{i-1}\Delta_i}\left(Gh'\right)_i-\frac{\Delta_i}{\Delta_{i-1}}\left(Gh'\right)_{i-1/2}\right] \tag{68}$$

where $h'_{i+1/2}=(h_{i+1}-h_i)/\Delta_i$, analogously for $h'_{i-1/2}$, $G_{i\pm1/2}$ is evaluated on half-indices and h'_i is approximated using the scheme (67). The discretisation (68) is used to approximate the single-variable μ-derivative terms in the test particle operator if the Gauss–Laguerre grid is employed.

To approximate the μ-derivatives occurring in the mixed derivative terms in equation (46) we use the scheme given by (67); $v_\parallel$-derivatives on the uniform $v_\parallel$ grid are discretised using the standard centered difference.

The discretisation of the test-particle operator on the non-uniform μ-grid thus obtained does not ensure exact self-adjointness and density conservation of the test-particle operator because discrete counterparts of the fundamental theorem of calculus and integration by parts are no longer satisfied. Density conservation and self-adjointness are therefore only approximate and improve with increased resolution. We show in the following section how exact density conservation can be restored on a non-uniform grid and examine the implication of non-exact self-adjointess for entropy production. Exact density conservation and self-adjointness can in principle also

be obtained on non-uniform grids by using a discretisation scheme that includes the integration weights, albeit at the expense of higher-order accuracy of the discretisation [4].

3.1.3. Discretisation matrix. To facilitate numerical implementation we now construct a discretisation matrix for the test particle operator. The single-variable $v_\parallel-$ and $\mu-$differential terms can be represented in discretized velocity-space using N_μ and $N_{v_\parallel}$ tridiagonal matrices, respectively, with dimensions $N_{v_\parallel} \times N_{v_\parallel}$ for the $v_\parallel-$operator and $N_\mu \times N_\mu$ for the $\mu-$operator. We denote these matrices as $C_{v_\parallel''}$ and $C_{\mu''}$. For the mixed-differential components of the test particle operator we define the tridiagonal operators $C_\mu[\cdot] := \partial/\partial\mu[\cdot]$ and $\widetilde{C}_\mu[\cdot] := \partial/\partial\mu[v_\parallel \mu\nu_x F_0 \cdot]$, and analogously $C_{v_\parallel}[\cdot] := \partial/\partial v_\parallel[\cdot]$ and $\widetilde{C}_{v_\parallel}[\cdot] = \partial/\partial v_\parallel[v_\parallel \mu\nu_x F_0 \cdot]$. The distribution function is represented by a matrix $h \in \mathbb{R}^{N_{v_\parallel} \times N_\mu}$. The combined mixed-differential operator, $C_{v_\parallel \mu}$, acting on $h^T \in \mathbb{R}^{N_\mu \times N_{v_\parallel}}$—the choice to operate on the transpose h^T will be motivated shortly—can then be written as

$$C_{v_\parallel \mu}\left[h^T\right] = C_\mu h^T \widetilde{C}^T_{v_\parallel} + \widetilde{C}_\mu h^T C^T_{v_\parallel}. \tag{69}$$

With $vec(ABC) = (C^{\mathrm{T}} \otimes A) vec(B)$, where $\otimes$ denotes the Kronecker product, one obtains

$$vec\left(C_{v_\parallel \mu}\left[h^T\right]\right) = \left[\widetilde{C}_{v_\parallel} \otimes C_\mu + C_{v_\parallel} \otimes \widetilde{C}_\mu\right] vec\left(h^T\right), \tag{70}$$

where $vec(h^T)$ is a $N_\mu N_{v_\parallel} \times 1$-column vector obtained by stacking the columns of h^T. It is straightforward to verify that the individual mixed-differential operators are not self-adjoint but when taken together satisfy this property. Accordingly, for uniform grids, where self-adjointness is exact, the discretisation matrix of the combined mixed differential operators, shown in figure 3(a), is exactly symmetric. Combining the mixed-differential terms with the single variable terms, the test particle operator is represented by the matrix

$$\begin{aligned} C_{\mathrm{test}} = {} & \widetilde{C}_{v_\parallel} \otimes C_\mu + C_{v_\parallel} \otimes \widetilde{C}_\mu \\ & + I_{v_\parallel} \otimes C_{\mu''} + C_{v_\parallel''} \otimes I_\mu, \end{aligned} \tag{71}$$

where $I_{v_\parallel} \in \mathbb{R}^{N_{v_\parallel} \times N_{v_\parallel}}$ and $I_\mu \in \mathbb{R}^{N_\mu \times N_\mu}$ denote identity matrices. The matrix C_{test} has dimension $N_\mu N_{v_\parallel} \times N_\mu N_{v_\parallel}$ and is block-tridiagonal, with nine non-zero bands and upper and lower bandwidth $w = N_\mu + 1$. The choice to operate on h^T yields a bandwidth $w = N_\mu + 1$, whereas an operator that acts on h results in a bandwidth $w = N_{v_\parallel} + 1$. Since typically in `stella` the number of $v_\parallel$-grid points exceeds the number of μ-grid points, we chose to operate on h^T to obtain a lower bandwidth. The structure of the matrix is shown in figure 3, for $N_\mu = 4$ and $N_{v_\parallel} = 8$. The symmetry of the matrix reflects the exact self-adjointness of the test-particle operator on uniform grids. Individual blocks describe the μ-discretisation and are tridiagonal. The matrix C_{test} is stored in a compact band format in `stella`; vanishing elements outside the bandwidth of C_{test} are not required.

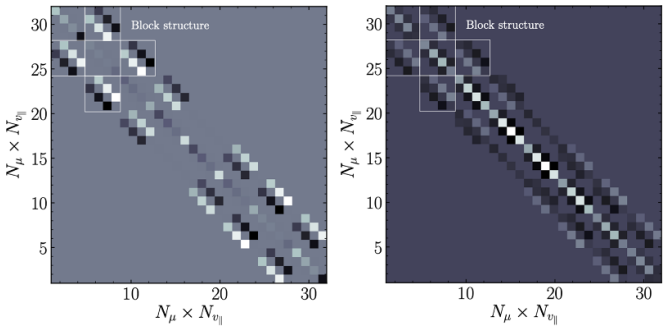

Figure 3. Discretisation matrices of the test-particle operator for $(N_\mu = 4, N_{v_\parallel} = 8)$: Left: structure of the combined mixed-differential terms that, taken together, are symmetric. Right: full block-tridiagonal symmetric discretisation matrix of the test particle operator. Blocks have dimension $N_\mu \times N_\mu$ and are tridiagonal. The matrix has upper and lower bandwidth $w = N_\mu + 1$, elements outside the band-width vanish.

3.2. Time advance

The diffusive terms in the test particle operator result in a Courant-Friedrichs-Levy (CFL) timestep constraint that scales with the square of the velocity discretisation size if an explicit time advance scheme is used. Even for a modest collisionality, this can be impractical. To avoid this constraint, the collision operator is implemented in `stella` using an implicit time advance scheme. We make use of Godunov splitting to separate the collisional time advance from the remainder of the gyrokinetic equation [see 4]. Using the backward Euler method one obtains

$$\begin{aligned} \frac{g_s^{n+1} - g_s^*}{\Delta t} &= C_{\mathrm{GK}}\left[h_s^{n+1}\right] \\ &= C_{\mathrm{test}}\left[h_s^{n+1}\right] + C_{\mathrm{field}}\left[h_s^{n+1}, h_{s'}^{n+1}\right] \end{aligned} \tag{72}$$

where s denotes the species index, g_s^* denotes the guiding centre distribution function after advancing the non-collisional part of the gyrokinetic equation, and h_s^{n+1} denotes the non-Boltzmann distribution function after the collisional time advance. In equation (72), the test-particle operator, $C_{\mathrm{test}}[h_s^{n+1}]$, contains self-collisions and inter-species collisions, but acts only on h_s; the contributions from different species are therefore collected into a single operator. The field-particle operator acts on h_s and all other species $h_{s'}$. With $g_s^{n+1} = h_s^{n+1} + (q_s/T_s) J_{0s} \phi^{n+1} F_{0s}$ it follows that the equation for the species h_s is

$$\begin{aligned} (1 - \Delta t C_{\mathrm{test}})\, h_s^{n+1} = {} & g_s^* + \frac{q_s}{T_s} J_{0s} \phi^{n+1} F_{0s} \\ & + \Delta t C_{\mathrm{field}}\left[h_s^{n+1}, h_{s'}^{n+1}\right]. \end{aligned} \tag{73}$$

Note that we have suppressed spectral indices, and used that the gyroaverage of the electrostatic potential is simply $J_{0s}(k_\perp v_\perp/\Omega_s)\phi_{\boldsymbol{k}_\perp}$ in Fourier space. Equation (73) is linear in h_s and can be split into a homogeneous and inhomogeneous component

$$(1-\Delta t C_{\text{test}})\, h_{s,inh}^{n+1} = g_s^* \tag{74}$$

$$(1-\Delta t C_{\text{test}})\, h_{s,hom}^{n+1} = \frac{q_s \phi^{n+1}}{T_s} J_{0s} F_{0s} + \Delta t C_{\text{field}}\left[h_s^{n+1}, h_{s'}^{n+1}\right], \tag{75}$$

with $h_s = h_{s,hom} + h_{s,inh}$. The first, inhomogeneous equation—so called because the right-hand-side depends on the intermediate timestep—can be solved for $h_{s,inh}^{n+1}$ by LU-factorisation of $R = 1 - \Delta t C_{\text{test}}$ and backsubstitution. We use `LAPACK`'s [3] `zgbtrs` algorithm for banded matrices to perform the LU-factorisation of R.

The second, homogeneous equation depends only on quantities at the new timestep $n+1$ and includes the field associated with the electrostatic potential and an additional field for every term in the Hirshman-Sigmar expansion of the field particle operator. Equation (75) is solved using a Green's function method: A unit impulse is supplied to the electrostatic potential and $[1-\Delta t C_{\text{test}}] h_{s,hom} = q_s J_0 F_{0s}/T_s$ is solved to obtain the response $\delta h_{hom,\phi}/\delta\phi$; analogously for each field ψ_j^{lm} appearing in the field-particle operator in equation (75), the equation $[1-\Delta t C_{\text{test}}] h_{s,hom} = \Delta t P_{lm} J_m \Delta_j^{(lm)}$ is solved for the response $\delta h_{s,hom}/\delta \psi_j^{lm,ss'}$, where we have subsumed multiplicative constants from the field-particle operator into $\Delta_j^{(lm)}$ for brevity. Here, all quantities are understood to be taken at the timestep $n+1$. With the responses in hand, the homogeneous solution at the new timestep $n+1$ is given by

$$h_{s,hom}^{n+1} = \phi^{n+1} \frac{\delta h_{s,hom}}{\delta \phi} + \sum_{jlm,s'} \psi_{j,lm}^{ss',n+1} \frac{\delta h_{s,hom}}{\delta \psi_{j,lm}^{ss'}}, \tag{76}$$

as can be verified by operating on the equation with $1-\Delta t C_{\text{test}}$. The summation runs over all species, s', and all expansion indices j, l and m. The electrostatic potential is related to the distribution function via the quasi-neutrality operator [5]

$$\begin{aligned}\phi = Q[h_s] &:= \frac{1}{\sum_s \frac{Z_s^2}{T_s}(\Gamma_{0s}-1) n_s} \sum_s Z_s n_s \frac{2B}{\pi^{1/2}} \int J_{0,s} h_s \, \mathrm{d}^3 v \\ &= \sum_s Q_s[h_s] \end{aligned} \tag{77}$$

where s denotes the species index, $\Gamma_{0s} := \exp(-k_\perp^2 \rho_s^2/2) I_0(k_\perp^2 \rho_s^2/2)$, I_0 is the modified Bessel function of the first kind, and equation (77) defines the per-species quasineutrality operators $Q_s[h_s] =: \phi_s$. Operating with Q_s on equation (76) one obtains

$$\phi_{s,hom}^{n+1} = \phi_s Q_s\left[\frac{\delta h_{s,hom}}{\delta\phi}\right] + \sum_{jlm,s'} \psi_{j,lm}^{ss',n+1} Q_s\left[\frac{\delta h_{s,hom}}{\delta \psi_{j,lm}^{ss'}}\right]. \tag{78}$$

Recalling the results from section 2.2, the fields in the field particle operator are obtained via

$$\begin{aligned}\psi_{j,lm}^{ss'} = P_{j,lm}^{ss'}[h_{s'}] := c_{l,-m} \frac{(-1)^m}{N_j^{(l)}} \int P_{l,-m} J_m \\ \times h_{s'} \Delta_j^{l,s's} \left(x_s^l L_j^{\left(l+\frac{1}{2}\right)}\left(x_s^2\right) F_{0s}\right) \mathrm{d}^3 v \end{aligned} \tag{79}$$

where we have defined the integral operator $P_{j,lm}^{ss'}$. Operating with $P_{j,lm}^{s's}$ on equation (76) one obtains

$$\begin{aligned}\psi_{j,lm,hom}^{s's,n+1} = \phi^{n+1} P_{j,lm}^{s's}\left[\frac{\delta h_{s,hom}}{\delta\phi}\right] \\ + \sum_{ipq,s''} \psi_{i,pq}^{ss'',n+1} P_{j,lm}^{s's}\left[\frac{\delta h_{s,hom}}{\delta \psi_{i,pq}^{ss''}}\right]. \end{aligned} \tag{80}$$

With $h_{s,inh}^{n+1}$ known from solving the inhomogeneous equation (74), $\phi_{inh}^s = Q_s[h_{s,inh}]$ and $\psi_{j,lm,inh}^{s's} = P_{j,lm}^{s's}[h_{s,inh}]$ we have obtained a linear system of equations for the potential $\phi^{n+1} = \sum_s (\phi_{s,inh}^{n+1} + \phi_{hom}^{s,n+1})$ and the fields $\psi_{j,lm}^{ss',n+1}$ at the new timestep $n+1$, given by

$$[\boldsymbol{I} - \boldsymbol{R}]\, \boldsymbol{f}^{n+1} = \boldsymbol{f}_{inh}^{n+1} \tag{81}$$

where $\boldsymbol{f}^{n+1} = [\phi^{n+1}, \{\psi_{j,lm}^{ss',n+1}\}]^T$, $\boldsymbol{f}_{inh}^{n+1} = [\phi_{inh}^{n+1}, \{\psi_{j,lm,inh}^{ss',n+1}\}]^T$ and $\boldsymbol{I}$ is the identity matrix. For the case of two species s and s', the matrix $\boldsymbol{R}$ is given by

$$\boldsymbol{R} = \begin{bmatrix} Q\left[\delta h^{\phi}\right] & Q_s\left[\delta h_s^{\psi_{jlm}^{ss}}\right] & Q_s\left[\delta h_s^{\psi_{jlm}^{ss'}}\right] & Q_{s'}\left[\delta h_{s'}^{\psi_{jlm}^{s's}}\right] & Q_{s'}\left[\delta h_{s'}^{\psi_{jlm}^{s's'}}\right] & \cdots \\ P_{jlm}^{ss}\left[\delta h_s^{\phi}\right] & P_{jlm}^{ss}\left[\delta h_s^{\psi_{jlm}^{ss}}\right] & P_{jlm}^{ss}\left[\delta h_s^{\psi_{jlm}^{ss'}}\right] & 0 & 0 & \\ P_{jlm}^{ss'}\left[\delta h_{s'}^{\phi}\right] & P_{jlm}^{ss'}\left[\delta h_s^{\psi_{jlm}^{ss}}\right] & P_{jlm}^{ss'}\left[\delta h_s^{\psi_{jlm}^{ss'}}\right] & 0 & 0 & \\ P_{jlm}^{s's}\left[\delta h_s^{\phi}\right] & 0 & 0 & P_{jlm}^{s's}\left[\delta h_{s'}^{\psi_{jlm}^{s's}}\right] & P_{jlm}^{s's}\left[\delta h_{s'}^{\psi_{jlm}^{s's'}}\right] & \\ P_{jlm}^{s's'}\left[\delta h_{s'}^{\phi}\right] & 0 & 0 & P_{jlm}^{s's'}\left[\delta h_{s'}^{\psi_{jlm}^{s's}}\right] & P_{jlm}^{s's'}\left[\delta h_{s'}^{\psi_{jlm}^{s's'}}\right] & \\ \vdots & & & & & \ddots \end{bmatrix} \tag{82}$$

where we have adopted the shorthand $\delta h_s^{\psi_{jlm}^{ss}} := \delta h_s / \delta \psi_{jlm}^{ss}$ for the responses, and for brevity the matrix above shows only one combination of the indices j, l and m. The response matrix $\boldsymbol{R}$ has dimension $(1+N_j N_l^2) \times (1+N_j N_l^2)$.

The LU-factorisation of $\boldsymbol{R}$ can be pre-computed at code initialisation, since all quantities occurring in the response matrix are time-independent. The linear system (81) can then be solved for the fields $\{\phi^{n+1}, \psi_{j,lm}^{ss',n+1}\}$ at every timestep by backsubstitution. With the fields $\{\phi^{n+1}, \psi_{j,lm}^{ss',n+1}\}$ computed, the implicit time advance equation (73) is solved for the distribution function at the new timestep, h^{n+1}.

3.3. Conservation properties

3.3.1. Exact density conservation on non-uniform grids. It can be shown that the first ($l=0$, $j=1$)- and ($l=1$, $j=0$)-terms in the field-particle operator expansion correspond to energy and momentum conserving operators, respectively, that exactly compensate the energy and momentum production of the test particle operator [see 1, 13], such that both quantities are conserved by the full collision operator. To guarantee the conservation of density, momentum and energy to machine precision, care must be taken in performing the discretisation of the test particle operator and the numerical calculation of integrals in the field particle operator. Density conservation of the test particle operator is guaranteed if the uniform velocity grid and uniform integration weights are employed. In the case of the μ-grid chosen by Gauss–Laguerre quadrature, the density moment of the test-particle operator vanishes only approximately, and density conservation is dependent on the velocity space resolution. We can nonetheless enforce exact conservation of density by the full collision operator by introducing an additional term in the field particle operator, $F_{0s}^* \psi_{j=0}^{s,l=0,*}$, with

$$F_{0s}^* \psi_{j=0}^{s,l=0,*} = F_{0s}^* \frac{\int \sum_{s'} C_{\text{test}}^{ss'}[h_{s'}] \, \mathrm{d}^3 v}{\int F_{0s}^* \, \mathrm{d}^3 v}, \tag{83}$$

where the sum over s' accounts for contributions from like-species and interspecies collisions. The numerator in (83) accounts for the total density of species s that is artificially produced in collisions with species s' due to inexact numerical density conservation. Since the density moment of the test-particle operator is approximately zero, the term $F_{0s}^* \psi_{j=0}^{s,l=0,*}$ is a small correction to the collision operator. The function F_{0s}^* must be chosen so that momentum and energy conservation of the total collision operator remain intact. With

$$F_{0s}^* = F_{0s} - v^2 F_{0s} \frac{\int v^2 F_{0s} \, \mathrm{d}^3 v}{\int v^4 F_{0s} \, \mathrm{d}^3 v} \tag{84}$$

where F_{0s} is the Maxwellian, this is guaranteed since the parallel momentum and energy moments of F_{0s}^* vanish, independent of the numerical integration scheme so long as integrals are calculated consistently using the same numerical scheme. With the addition of the small correction term (83) to the field-particle operator, we can enforce exact density conservation of the collision operator on non-uniform velocity grids.

Density conservation of the field particle operator is automatically satisfied for terms in the operator that are odd in $v_\parallel$, since `stella` employs a grid for integration in $v_\parallel$ that is anti-symmetric around $v_\parallel = 0$. For even terms, exact density conservation is not guaranteed. To enforce this for the energy restoring term $\{l=0, j=1\}$ one can make the modification

$$\Delta_{j=1}^{l,ss'} \longrightarrow \Delta_{j=1}^{l,ss'} - \frac{F_{0s}^*}{\int F_{0s}^* \, \mathrm{d}^3 v} \int \Delta_{j=1}^{l,ss'} \, \mathrm{d}^3 v, \tag{85}$$

to ensure conservation of number density to machine precision. The modification (85) remains accurate as long as the integral over $\Delta_{j=1}^{l,ss'}$ is small; in numerical tests the modification incurs at worst a 10% error, in the case of disparate mass ratios $\mu \leqslant 10^{-4}$ at the default velocity space resolution.

3.3.2. Exact momentum and energy conservation. Interspecies momentum conservation requires that for $k_\perp = 0$

$$\int m_s v_\parallel C_{\text{test}}^{ss'}[h_s] \, \mathrm{d}^3 v = -\int m_{s'} v_\parallel C_{\text{field}}^{s's}[h_s] \, \mathrm{d}^3 v. \tag{86}$$

Using $P_{l=1}^{m=0}(\cos\theta) = v_\parallel / v$, the self-adjointness of $\Delta_j^{ss'}$ and $\int v_\parallel^2 / v^2 f(v) \mathrm{d}^3 v = \int \cos^2(\theta) \sin\theta \mathrm{d}\theta \int f(v) v^2 \mathrm{d}v = 2/3 \int f(v) v^2 \mathrm{d}v = \frac{1}{3} \int f(v) \mathrm{d}^3 v$, one obtains

$$\begin{aligned} &\int m_s v_\parallel C_{\text{test}}^{ss'}[h_s] \, \mathrm{d}^3 v \\ &\quad = -m_{s'} \int \frac{h_s}{F_{0s}} \times \frac{v_\parallel}{v} \Delta_{j=0}^{l=1,ss'}[v F_{0s'}] \, \mathrm{d}^3 v. \end{aligned} \tag{87}$$

For this condition to be satisfied to machine precision we use that $\Delta_{j=0}^{ss',l=1}$ can be expressed using the test-particle operator. A straightforward calculation shows that

$$\Delta_{j=0}^{ss',l=1}\left[x_{s'} \exp\left(-x_{s'}^2\right)\right] = \mu_{ss'}^2 x_s \nu_S^{ss'}(x_s) \exp\left(-x_s^2\right) \tag{88}$$

where ν_S is the slowing-down frequency from the test particle operator. Using the identity (88) and the differential identities from Abel *et al* [1] yields

$$\frac{v_\parallel}{v} \Delta_{j=0}^{ss',l=1}(x_{s'} F_{0s'}) = \frac{1}{v_{th,s}} \frac{m_s}{m_{s'}} C_{\text{test}}^{ss'}\left[v_\parallel F_{0s}\right]. \tag{89}$$

In the numerical implementation of the field particle operator we can therefore compute $\Delta_{j=0}^{l=1,ss'}$ using (89) to guarantee exact momentum conservation (86) so long as the test-particle operator satisfies exact self-adjointness, which is the case if uniform velocity grids are employed. To ensure exact momentum conservation on non-uniform velocity grids, we can replace the field particle term with the integral moment of the test particle operator using (86). This comes at an additional computational cost since the test-particle operator acting on h_s in (86) must be evaluated before the integral is computed.

Energy conservation can be treated analogously. Conservation to machine precision requires

$$\int m_s v^2 C_{\text{test}}^{ss'}[h_s] \, \mathrm{d}^3 v = -\int m_{s'} v^2 C_{\text{field}}^{s's}[h_s] \, \mathrm{d}^3 v. \tag{90}$$

Writing out the $\Delta_{j=1}^{ss',l=0}$-term of the field particle operator on the right-hand-side gives

$$\int m_s v^2 C_{\text{test}}^{ss'}[h_s]\ \mathrm{d}^3v = m_{s'}\int \frac{h_s}{F_{0s}} \times \Delta_{j=1}^{ss',l=0}\left[\left(3/2-x_{s'}^2\right)F_{0s'}\right]\ \mathrm{d}^3v. \quad (91)$$

Relating $\Delta_{j=1}^{ss',l=0}$ to the collision frequencies occurring in the test particle operator yields

$$\Delta_{j=1}^{ss',l=0}\left[\left(3/2-x_{s'}^2\right)\exp\left(-x_{s'}^2\right)\right] = -\mu_{ss'}^{3/2}x_s^2\nu_E^{ss'}(x_s)\exp\left(-x_s^2\right). \quad (92)$$

Again using the differential identities of Abel *et al* [1] for the collision frequencies occurring in the test-particle operator it follows that

$$\Delta_{j=1}^{ss',l=0}\left[\left(3/2-x_{s'}^2\right)F_{0s'}\right] = C_{\text{test}}^{ss'}\left[m_s v^2 F_{0s}\right]. \quad (93)$$

Equation (93) can then be employed to calculate $\Delta_{j=1}^{ss',l=0}$ using the test-particle operator so that exact conservation of energy is ensured if the test-particle operator satisfies exact self-adjointness. On non-uniform grids, where this is not the case, one may use (90) directly to evaluate the energy-conserving term in the field-particle operator, again, at the additional computational expense of calculating the test particle operator acting on h_s.

4. Numerical tests

4.1. Conservation properties

We first test the conservation properties of the collision model implemented in `stella`. The conversion of the collision operator into the gyrokinetic form introduced spatial dependencies via the gyrodiffusive term and Bessel functions; as a result the first three velocity moments no longer vanish when $k_\perp \neq 0$. Abel *et al* [1] and Barnes *et al* [4] have shown that the conservation laws for the gyrokinetic collision operator can be expressed as a condition on the collision operator in the limit $k_\perp = 0$, namely, requiring

$$\int \left(1, v_\parallel, v^2\right)^T C_{\text{GK},k_\perp=0}[h_{\boldsymbol{k}}]\ \mathrm{d}^3v = 0 \quad (94)$$

ensures that density, momentum and energy are locally conserved by the collision operator [1]. Here $C_{\text{GK},k_\perp=0}$ denotes the gyrokinetic collision operator with all finite Larmor radius terms of the operator disabled in both the test and field particle components [see 1]. For the collision model implemented in `stella`, by construction, this condition is satisfied if the $(j=1,l=0)$- and $(j=0,l=1)$-terms are retained in the spherical harmonic and Hirshman-Sigmar expansion of the field-particle operator. To test that these conservation properties indeed hold for the numerical implementation of the collision

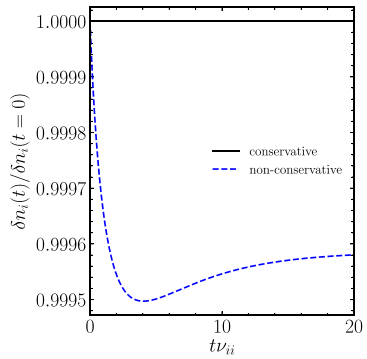

Figure 4. Evolution of the perturbed ion density due to the collision model in the limit $k_\perp = 0$, over 20 collision times (dashed blue line). The distribution function was initialised as defined in equation (95). Using uniform grids or including the density restoring term on the non-uniform μ-grid ensures density conservation to machine precision (continuous black line).

model, the distribution function was initialised with non-zero density, momentum, and energy moments as

$$h\left(v_\parallel,\mu\right) = \left[1+\frac{mv_\parallel}{T_0}\delta u_{\parallel,0}+\left(\frac{mv_\parallel^2}{T_0}-\frac{1}{2}\right)\frac{\delta T_{\parallel,0}}{T_0}\right]F_{0s} \quad (95)$$

where $\delta u_{\parallel,0}$ and $\delta T_{\parallel 0}$ are constants. All non-collisional terms in the gyrokinetic equation were disabled. The evolution of the density, momentum and energy was then measured over 20 collision times, $\tau_{ii} = \nu_{ii}^{-1}$, shown in figures 4 and 5, with and without the conserving terms in the collision operator. Density conservation to machine precision was verified for uniform velocity space grids, where the integration weights are equal to the inverse grid spacing. For the μ-grid initialized by Gauss–Laguerre quadrature a density decay of $1-\delta n_i(20\tau_{ii})/\delta n_i(t=0) \sim 10^{-3}$ is observed. Thus, as expected, density is only approximately conserved on this non-uniform grid. Inclusion of the density correction term (83) in the field particle operator was verified to recover density conservation to machine precision on `stella`'s non-uniform μ-grid.

Figure 5 shows that the parallel momentum and energy decay significantly over 20 collision times in the absence of the field particle operator. Inclusion of the $(j=0,l=1,m=0)$-term in the field particle operator, calculated as prescribed in the previous section, leads to parallel momentum conservation to machine precision. Similarly, inclusion of the $(j=1,l=0,m=0)$-term ensures that energy is conserved. These tests verify that the numerical implementation of the collision model satisfies the required conservation laws.

4.2. H-theorem

Boltzmann's H-theorem mandates that the entropy production rate of the collision operator must be non-negative at all times and zero only if the distribution function is Maxwellian. To verify that this holds, the distribution function was initialised as random in velocity space, with $h(v_\parallel,\mu)$ drawn from the uniform distribution $U[-1/2,1/2]$, following Barnes *et al* [4]. Expanding the phase-space average of the entropy

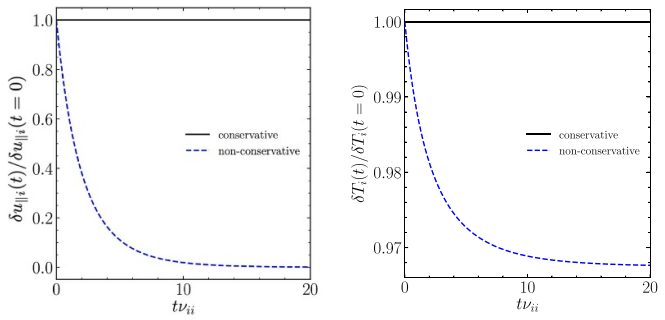

Figure 5. Evolution of the parallel flow (left) and energy (right) due to the collision model in the limit $k_\perp = 0$, over 20 collision times. The distribution function was initialised as defined in equation (95). Including the $(j=0, l=1, m=0)$ and $(j=1, l=0, m=0)$ terms of the field-particle operator ensures conservation of both quantities to machine precision (continuous black line).

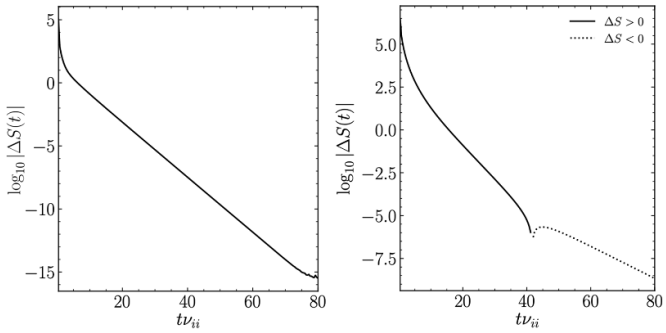

Figure 6. Rate of change of the entropy due to collisions. Left: entropy production for the numerical scheme that ensures exact self-adjointness of the collision operator on uniform velocity-space grids. The entropy production is always non-negative and approaches zero as the distribution function approaches a Maxwellian. Right: entropy production for the Gauss–Laguerre μ-grid on which the collision operator is only approximately self-adjoint. The entropy production is non-negative (solid line) and decays over 14 orders of magnitude as the distribution function approaches a Maxwellian, before small negative entropy production sets in (dotted line) that then decays.

$S = -\iint \frac{\mathrm{d}^3\boldsymbol{R}}{V} f \ln f \,\mathrm{d}^3 v$, the entropy of the fluctuating part of the distribution function is given by

$$S[\delta f] \approx -\iint \frac{\mathrm{d}^3\boldsymbol{R}}{V} \frac{\delta f^2}{2F_0} \,\mathrm{d}^3 v, \tag{96}$$

where we have retained only the lowest order term. The time evolution of the rate of change of S, $\mathrm{d}S/\mathrm{d}t \propto \Delta S = (S_{i+1} - S_i)$, where i denotes the timestep, is shown in figure 6. On `stella`'s uniform velocity grid, the entropy production rate is always positive and decays uniformly until it reaches machine precision $\sim 10^{-15}$ at $t\nu_{ii} = 80$, as is expected for a scheme that guarantees exact self-adjointness. On the μ-grid determined by Gauss–Laguerre quadrature, the entropy production rate is positive and decays over thirteen orders of magntitude as the distribution function approaches a Maxwellian in velocity space. At $\Delta S(t) \approx 10^{-6.5}$, negative entropy production sets in that then decays to $\Delta S(t) \approx 10^{-9}$ at $t\nu_{ii} = 80$. While satisfaction of the H-theorem is not guaranteed on non-uniform velocity grids, such small deviations are expected to be benign. If required, this can be verified by comparison with the uniform velocity grid.

4.3. Comparison with `GS2`

We next benchmark the implementation of the collision operator in `stella` against the collision model implemented in the gyrokinetic solver `GS2` [17]. The `GS2` collision model is described in detail in Barnes *et al* [4] and Abel *et al* [1]; we briefly recapitulate key features here: the code uses (E, λ)-velocity space coordinates, where E denotes the particle kinetic energy, and $\lambda := \mu/E$. The test-particle operator implemented in `GS2` consists of the standard pitch-angle scattering and energy diffusing operators described in the first section of this paper. The field particle operator implemented in `GS2` consists of two terms that ensure conservation of momentum and energy by the full collision operator. The energy-conserving term corresponds identically to the $(j=1, l=0)$-energy-conserving term of the collision model introduced here, and is given by [4]

$$E[h_{\boldsymbol{k}}] = v^2 \nu_E J_0(a) F_0 \frac{\int \nu_E v^2 J_0(a) h_{\boldsymbol{k}} \mathrm{d}^3 v}{\int \nu_E v^4 F_0 \mathrm{d}^3 v}. \tag{97}$$

where $a := k_\perp v_\perp / \Omega$ and species indices have been dropped everywhere for clarity. The pitch-angle scattering (Lorentz) and energy diffusing operators in `GS2` are implemented using an operator-splitting method; to ensure exact momentum conservation of each operator while retaining self-adjointness, the Lorentz operator is combined with a momentum conserving term given by [4]

$$U_L[h_{\boldsymbol{k}}] = \nu_D F_0 \left[J_0(a) v_\parallel \frac{\int \nu_D v_\parallel J_0(a) h_{\boldsymbol{k}} \mathrm{d}^3 v}{\int \nu_D v_\parallel^2 F_0 \mathrm{d}^3 v} + J_1(a) v_\perp \frac{\int \nu_D v_\perp J_1(a) h_{\boldsymbol{k}} \mathrm{d}^3 v}{\int \nu_D v_\parallel^2 F_0 \mathrm{d}^3 v} \right]. \tag{98}$$

To compensate momentum production by the energy diffusing term of the test particle operator, the field particle model of `GS2` includes the term

$$U_D[h_{\boldsymbol{k}}] = -\Delta\nu F_0 \left[J_0(a) v_\parallel \frac{\int \Delta\nu v_\parallel J_0(a) h_{\boldsymbol{k}} \mathrm{d}^3 v}{\int \Delta\nu v_\parallel^2 F_0 \mathrm{d}^3 v} + J_1(a) v_\perp \frac{\int \Delta\nu v_\perp J_1(a) h_{\boldsymbol{k}} \mathrm{d}^3 v}{\int \Delta\nu v_\parallel^2 F_0 \mathrm{d}^3 v} \right]. \tag{99}$$

Here the collision frequency $\Delta\nu := \nu_D - \nu_S$. The momentum conserving terms given by equations (98) and (99) resemble modifications of the momentum conserving term provided in Abel *et al* [1], that match the momentum conserving term implemented in `stella`. These modifications were made to ensure exact conservation and self-adjointness under `GS2`'s operator splitting method. With this in mind, we performed collisional gyrokinetic simulations in both codes to compare the collision operators implemented in `stella` and `GS2`.

Table 1. Parameters of linear Cyclone Base Case simulations with `stella` and `GS2`. The quantities r and R are the minor and major radius of the chosen flux surface of the DIII-D tokamak, respectively; q denotes the safety factor, $\hat{s}$ is the magnetic shear, κ is the flux surface elongation, δ the triangularity, a is the reference length, chosen to be the minor radius of the last-closed-flux-surface, and $v_{th,r}$ denotes the reference speed, chosen as $v_{th,r} = \sqrt{2T_{\mathrm{ref}}/m_{\mathrm{ref}}}$ with $T_{\mathrm{ref}} = T_i$ and $m_{\mathrm{ref}} = m_i$.

Cyclone Base Case parameters:	
$\tilde{r} = r/a$	0.5
$\tilde{R} = R_0/a$	2.77778
$\mathrm{d}\tilde{R}/\mathrm{d}\tilde{r}$	0.0
q	1.4
$\hat{s} = \mathrm{d}\ln q/\mathrm{d}\ln r$	0.8
κ	1.0
$\mathrm{d}\kappa/\mathrm{d}\tilde{r}$	0.0
δ	0.0
$\mathrm{d}\delta/\mathrm{d}\tilde{r}$	0.0
n_i/n_e	1.0
T_i/T_e	1.0
m_i/m_e	3672
$-\mathrm{d}\ln T_i/\mathrm{d}\tilde{r}$	2.49
$-\mathrm{d}\ln T_e/\mathrm{d}\tilde{r}$	2.49
$-\mathrm{d}\ln n_i/\mathrm{d}\tilde{r}$	0.8
$-\mathrm{d}\ln n_e/\mathrm{d}\tilde{r}$	0.8
Common simulation parameters:	
$\nu_{ii}a/v_{th,r}$	0.1
$\Delta t v_{th,r}/a$	0.008
$v_{c,\perp}/v_{th,s}$	3.0
$v_{c,\parallel}/v_{th,s}$	3.0
$N_{\mathrm{period}} \times N_z$	3×24
`stella` *simulation parameters:*	
μ-grid	Gauss-Quad.
$N_{v_\parallel}$	48
N_μ	12
`GS2` *simulation parameters:*	
N_{gauss}	20
N_E	32

4.4. Cyclone base case simulations

Linear gyrokinetic simulations of the Cyclone Base Case (CBC) regime of the DIII-D tokamak [8], a commonly used test-case for gyrokinetic codes, were first performed to benchmark the test-particle collision operator of `stella` against the operator implemented in `GS2`. The simulations were performed with kinetic ions; electrons were approximated to adiabatically stream along magnetic field lines, so that $\delta n_e = e n_{e0}\phi/T_e$. In `stella`, 24 grid-points in the field-line following coordinate z, 48 grid-points in $v_\parallel$ and 12 points in μ on a Gaussian grid were used. The code was evolved for 4000 time-steps with $\Delta t = 0.008 a/v_{th,i}$. In `GS2`, $n_\lambda = 33$ grid-points in λ, $n_E = 32$ grid-points in the energy coordinate and 24 grid-points in the field-line following coordinate were used. The velocity space cut-off speed was set to $v_{\parallel,c} = v_{\perp,c} = 3.0 v_{th,s}$ in `stella` and $v_c = 3.0 v_{th,s}$ in `GS2`. The simulation parameters are summarised in table 1.

Growth rate and frequency spectra obtained with both codes are shown in figure 7, for a non-collisional simulation ($\nu_{ii}a/v_{th,i} = 0$), and in figure 8 for a collisional simulation ($\nu_{ii}a/v_{th,i} = 0.1$) that employed only the test-particle operators in both codes. The inclusion of the test-particle component of the collision operator reduces the growth rates in both codes by 30%, from a maximum normalised growth rate of $\gamma a/v_{th,i} = \mathrm{Im}(\omega)a/v_{th,i} = 0.1$ at a wave number $k_y\rho_i = 0.55$ in the absence of collisions, to $\gamma a/v_{th,i} = 0.07$ at $k_y\rho_i = 0.55$ with strong test-particle collisions enabled. Excellent agreement of the growth rates and frequencies is obtained between both codes over the extent of the spectrum.

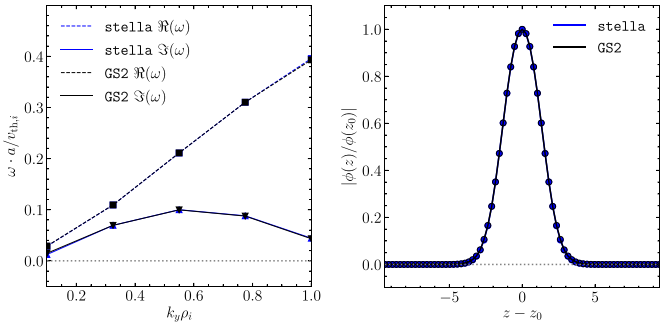

Figure 7. Left: Growth rates (solid lines) and real frequencies (dashed lines) for a collisionless ($\nu_{ii}a/v_{th,i} = 0.0$) Cyclone Base Case simulation, obtained using `GS2` (black) and `stella` (blue). Right: Electrostatic potential for the fastest growing mode ($k_y\rho_i = 0.55$) as a function of the parallel coordinate.

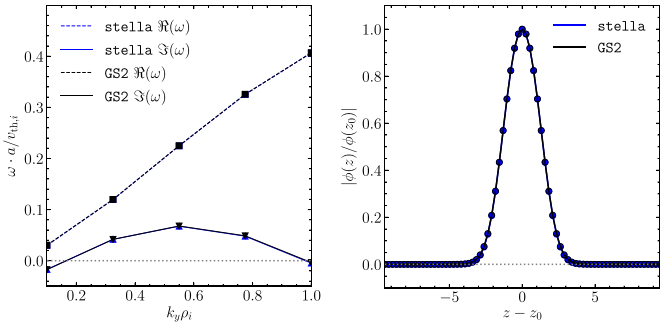

Figure 8. Left: Growth rates (solid lines) and real frequencies (dashed lines) for a collisional ($\nu_{ii}a/v_{th,i} = 0.1$) Cyclone Base Case simulation, obtained using `GS2` (black) and `stella` (blue), with collision models restricted to the test particle operator. Right: Electrostatic potential for the fastest growing mode ($k_y\rho_i = 0.55$) as a function of the parallel coordinate.

Next, a comparison of the energy-diffusion and energy-conserving terms in `stella` and `GS2` was performed in a CBC setting. In `stella`, the Lorentz operator was suppressed in the collision model, and the field-particle operator was configured to only include the $\{j = 1, l = 0\}$-term associated with energy conservation. Analogously the Lorentz operator was disabled in `GS2` and terms associated with perpendicular momentum conservation of the energy diffusion operator were suppressed. The remaining components in the `GS2` collision operator are then energy diffusion and energy conservation terms. Growth rates and real frequencies for both codes are shown in figure 9(left plot), with excellent agreement over the spectrum.

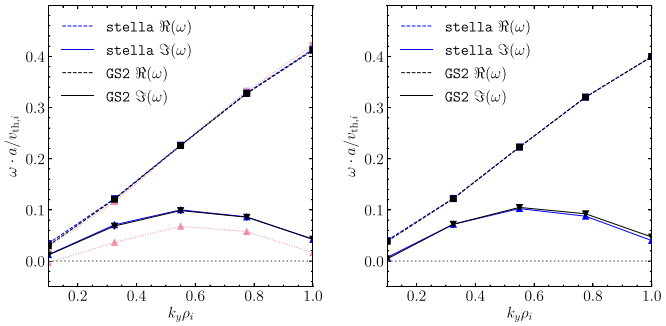

Figure 9. Left: Growth rates (solid lines) and real frequencies (dashed lines) for a collisional ($\nu_{ii}a/v_{th,i} = 0.1$) Cyclone Base Case simulation with only energy diffusion and energy-conserving terms included in the collision operator, obtained using `GS2` (black) and `stella` (blue). Growth rates and frequencies for an energy diffusion operator without the energy-conserving term are shown for comparison (red dotted line). Right: Growth rates and real frequencies for the full test-particle operator and energy and momentum conserving terms in both codes. The small discrepancy at $k_y\rho_i \sim 1$ is associated with a modification of the perpendicular momentum conserving terms made in the collision operator of `GS2`.

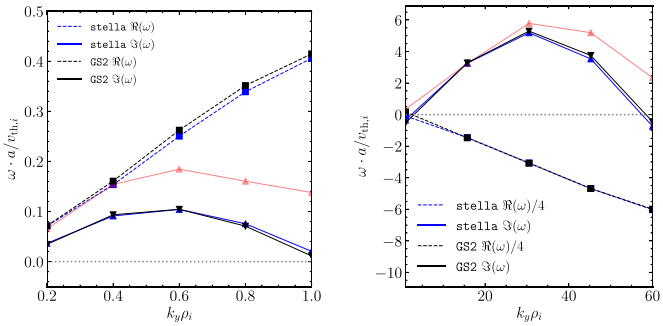

Figure 10. Left: Growth rates (solid lines) and real frequencies (dashed lines) for a collisional ($\nu_{ii}a/v_{th,i} = 0.1$, $\nu_{ee}a/v_{th,i} = 6.06$) CBC simulation with kinetic ions and electrons, on ion scales. Right: Growth rates and real frequencies on electron scales. Growth rates for a non-collisional simulation are shown for comparison in red.

Figure 9(right plot) shows the frequency and growth rate spectra when the momentum conserving terms in the field particle operator are included in `GS2` and `stella`. Good agreement is obtained at low $k_\perp\rho_i$ but a small discrepancy is found at $k_\perp\rho_i \sim 1$. We attribute this discrepancy to the modification, made for numerical purposes, of the momentum conserving terms in `GS2` described previously. The disagreement is more pronounced at $k_\perp\rho_i \sim 1$ because the Bessel function $J_1(a)$, occurring in the perpendicular momentum conserving terms in equations (98) and (99) are $J_1(a) \sim 1$ for $a \sim 1$ while $J_1(a) \to 0$ for $a \to 0$, where the argument of the Bessel function is given by $a = k_\perp v_\perp/\Omega$. The parallel momentum conserving terms in (98) and (99) are small for the CBC simulations performed here because the distribution function was approximately symmetric in $v_\parallel$; the integrals in the parallel momentum conserving terms, that are odd in $v_\parallel$, are then small.

Simulations of the CBC were also performed with both ion and electron species treated kinetically, to test interspecies collision terms. Because the Spitzer collisionality scales with the inverse square root of the species mass, the electron collision frequency exceeds the ion collision frequency by a factor $(m_i/m_e)^{1/2} = 60.6$ for a deuterium plasma; accordingly the simulations were performed with $\nu_{ii}a/v_{th,i} = 0.1$ and $\nu_{ee}a/v_{th,i} = \nu_{ei}a/v_{th,i} = 6.06$. For interspecies collisions, the collision model in `GS2` makes use of a mass-ratio expansion to discard ion-electron test-particle collisions and electron-ion energy diffusion; the Lorentz operator is further simplified by utilizing a mass ratio expansion to approximate the electron-ion deflection frequency with $\nu_D^{ei}(v) = \nu_{ei}(v_{th,e}/v)^3$ [see 1, 4]. We note that while a mass ratio expansion of the collision operator as employed in `GS2` is acceptable for very disparate species masses, this inevitably is inaccurate for collisions between ion species that have comparable masses, such as Deuterium and Tritium species. The collision model in `stella` makes no mass-ratio approximations for inter-species collisions, and for the kinetic two-species CBC simulations was configured to include all inter-species and energy- and momentum-conserving terms. A comparison of the growth rates and frequencies obtained with both codes for ion-scale wavenumbers, $k_y\rho_i \lesssim 1$, is shown in figure 10(left sub-figure), demonstrating good agreement between the codes. Growth rates and frequencies on electron scales $k_y\rho_i \lesssim 60$ are shown in figure 10(right sub-figure), also demonstrating good agreement throughout the spectrum.

The benchmarks performed against `GS2` described here verify the integrity of `stella`'s collision model when this is reduced to the basic test-particle and energy- and momentum-restoring field particle terms. We proceed to test the accuracy of higher-order terms in the field-particle operator implemented in `stella`.

5. Spitzer-Härm problem

To investigate the accuracy of the full collision model implemented in `stella`, we solve the time independent parallel Spitzer-Härm problem, that describes the electron response to a constant applied electric field and pressure and temperature gradients. To do so, all non-collisional terms in the gyrokinetic equation were disabled, and momentum and energy flux source terms associated with an applied parallel electric field and pressure and temperature gradients were introduced. The Spitzer problem then consists in solving

$$C_{ee}[f_e] + C_{ei}[f_e, f_{0i}] = -\left[v_\parallel \underbrace{\left(\frac{q_e E_\parallel}{T_e} - \nabla_\parallel \ln p_{0e} \right)}_{=:I_1} + v_\parallel \left(x_e^2 - \frac{5}{2} \right) \underbrace{[-\nabla_\parallel \ln T_{0e}]}_{=:I_2} \right] F_{0e} \tag{100}$$

for the electron distribution function, f_e, where we have defined the thermodynamic forces I_1 and I_2, and $x_e := v/v_{th,e}$. The linearity of equation (100) implies that the parallel particle and heat fluxes can be expressed as linear combinations of the thermodynamic forces [see 12] as

$$\frac{4m_e\tau_{ei}^{-1}}{3\sqrt{\pi}n_{0e}T_{0e}}\int v_{\|}f_e\,\mathrm{d}^3v = L_{11}I_1 + L_{21}I_2 \tag{101}$$

and

$$\frac{4m_e\tau_{ei}^{-1}}{3\sqrt{\pi}n_{0e}T_{0e}}\int v_{\|}\left(x_e^2-\frac{5}{2}\right)f_e\,\mathrm{d}^3v = L_{12}I_1 + L_{22}I_2, \tag{102}$$

respectively. Here, the coefficients L_{11}, L_{12}, L_{21} and L_{22} denote the Spitzer transport coefficients [see 7, 12], and

$$\tau_{ei}^{-1} = \frac{\sqrt{2}\pi\, q_e^2 q_i^2 n_{0i}\ln\Lambda}{m_e^{1/2}T_{0e}^{3/2}}. \tag{103}$$

To solve the time independent Spitzer problem with `stella`, the code was initialized to take a single timestep, Δt, that is large relative to the collision time, so that $\tau_c/\Delta t \to 0$. Setting independently first $I_1 = 0$ and then $I_2 = 0$, solving equation (100) with `stella` for both cases, and using equations (101) and (102), the transport coefficients L_{mn} can be calculated. For better accuracy of integral computations, the non-uniform μ-grid available in `stella` was used, at the expense of numerically exact conservation properties. Resolution scans were performed to determine that $n_{v_\|} = 72$ and $n_\mu = 46$ grid-points provide adequate velocity-space resolution. To evaluate the accuracy of the field particle model in `stella`, scans were then performed over the number of terms included in the field particle operator expansion. Errors in the Spitzer coefficients were calculated with respect to coefficients computed by Belli and Candy [7] using an implementation of the exact linearised Fokker–Planck operator in the neoclassical solver `NEO` [6]. The Spitzer coefficients calculated with `stella` for different configurations of the collision model and the coefficients obtained by Belli and Candy [7] are provided in table 2. Errors in the calculated Spitzer coefficients, relative to the exact coefficients, are shown in figure 11, as a function of successively higher-order terms retained in `stella`'s field particle operator. Using the collision model configured to include only the test-particle operator leads to significant errors in all three transport coefficients, as high as 50% in L_{11}. Further retaining the first two terms in the expansion of the field particle operator ($\{l=0, j=1\}, \{j=1, l=0\}$) – corresponding to the energy and momentum conserving collision model commonly used in gyrokinetic codes such as `GS2`—yields errors of $10\% - 25\%$ in the Spitzer coefficients. Including the next $\{j=1, l=1\}$ term associated with the collisional energy flux density reduces the errors in the coefficients to $1\% - 3\%$. Adding further higher-order terms, up to $\{j=2, l=1\}$, reduces the error in all three coefficients to less than 1%. In performing these scans, all m-indices associated with an individual l-index were included ($m \in \{-l, \ldots, l\}$). The Spitzer coefficients exhibit a symmetry $L_{12} = L_{21}$, known as Onsager symmetry [21], that is a consequence of the self-adjointess of the collision operator [12, see]. A comparison of the errors in L_{12} and L_{21} in figure 11 shows that Onsager symmetry holds approximately, as is expected by construction of the field-particle operator expansion (40) on a non-uniform velocity-space grid.

The scans performed in the Spitzer coefficients validate that the accuracy of the collision model implemented in `stella` can be increased progressively to rigorously approximate the exact linearised Fokker–Planck operator.

Table 2. Spitzer-Härm transport coefficients calculated with `stella` using only the test-particle operator (TPO), using the test-particle and momentum- and energy-conserving field-particle terms (+FP$_{\mathrm{EM}}$), and using additional terms up to the $j_1 l_1$-term in the field-particle operator (+FP$_{j_1 l_1}$). Coefficients calculated by Belli and Candy [7] using the exact linearized Fokker–Planck operator implemented in the neo-classical solver `NEO` (Exact) are provided for comparison.

Coefficient:	TPO:	+FP$_{\mathrm{EM}}$:	+FP$_{j_1 l_1}$:	Exact:
L_{11}	1.0019	1.7476	1.9632	1.9757
L_{12}	0.9181	1.4026	1.3861	1.3889
L_{21}	0.9243	1.0794	1.4171	1.3889
L_{22}	3.5229	4.0763	4.1859	4.1789

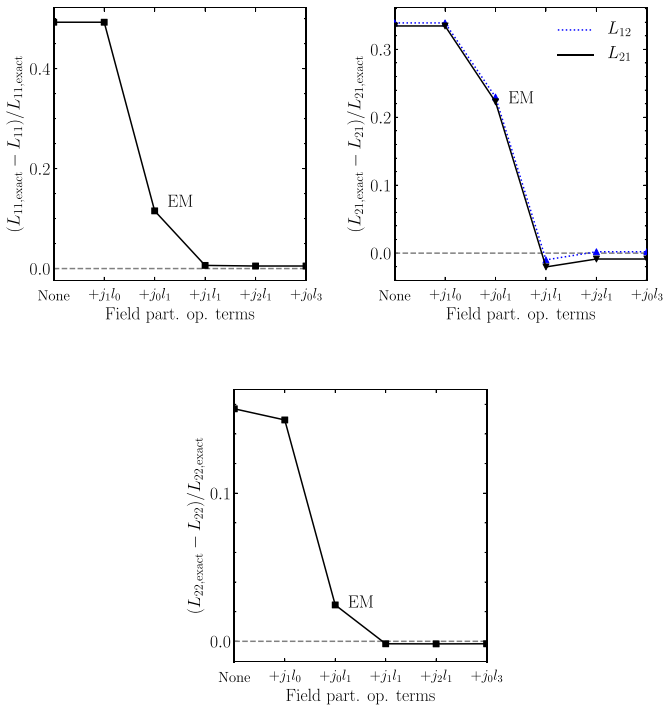

Figure 11. Errors in the Spitzer transport coefficients calculated with `stella`, relative to coefficients determined with the exact Fokker–Planck operator by Belli and Candy [7], for successively added terms in the field particle operator expansion. The energy and momentum conserving collision model (EM) corresponds to retaining all terms up to the $j=0$, $l=1$-term ('$j_0 l_1$') in the field-particle operator expansion. Including higher order terms in the field particle operator expansion up to $j=2$ and $l=1$ yields errors below 1% in all Spitzer coefficients.

6. Summary and future work

The collision model for the gyrokinetic solver `stella` presented in this work satisfies conservation laws and, uniquely, permits a rigorous approximation of the full linearised Fokker–Planck operator. Multiple plasma species are supported, with full intra- and inter-species collisions taken into account, irrespective of the species' mass ratio. In line with `stella`'s mixed implicit-explicit numerical scheme, the collision model makes use of an implicit algorithm to avoid a CFL constraint on the maximum timestep size. The diffusive, test-particle component of the linearised Fokker–Planck operator is treated exactly. The field-particle piece of the operator is approximated using series expansions in spherical harmonics and the Hirshman-Sigmar basis functions that are precomputed recursively from error functions during code initialisation. The expansion of the field-particle operator obtained in this way reduces the exact field-particle operator to an integral operator that can be treated implicitly using a Green's function method. In the limit where only the first two terms in the series expansion are retained, the collision model reduces to the energy- and momentum-conserving model commonly employed in gyrokinetic codes [see 1, 4, 25]. Benchmarks against the collision model of the gyrokinetic solver `GS2` for both ion- and electron scale turbulence confirm that this is the case. The classical Spitzer problem was then solved to test the implementation of higher-order terms in the Hirshman-Sigmar expansion. The results demonstrate the scalable accuracy of the collision operator: including the collisional energy-flux and higher-order terms in the field particle operator reduces errors in the Spitzer coefficients to under 1%, from errors in the 10%–50% range for simpler test particle or energy- and momentum-conserving collision models commonly employed in gyrokinetic codes. The algorithm introduced here therefore enables the user to perform numerical simulations with a collision model configured to meet the physical fidelity required by a given problem.

Accounting for collisional effects with high fidelity can, for instance, be important in simulations of trapped-electron mode instabilities and zonal flow (ZF) damping: work by Pan *et al* [22] with an exact, explicit implementation of the Fokker–Planck operator in the `GENE` code has demonstrated that an exact treatment of the field-particle operator results in significant corrections to instability growth rates and ZF damping in tokamaks [23], compared to a simpler energy- and momentum-conserving collision model. An accurate numerical treatment of collisions is also, inevitably, important for highly collisional phenomena, such as the transport of impurity species that have a significant collisionality due to their high ion charge. The transport of Carbon, Argon, Iron, or Tungsten impurities must be controlled in magnetic confinement reactors to avoid impurity accumulation in the plasma core, where highly charged species lead to a rapid radiative energy loss of the plasma. Measurements of the diffusion coefficients of iron ions, injected by laser ablation in W7-X, exceed neoclassical predictions by two orders of magnitude [10, 20], suggesting that turbulence plays an important role in the transport of these species. Indeed, gyrokinetic simulations of impurity transport in W7-X performed with `stella` [9] indicate that turbulence can explain the measured levels of transport—but these simulations have been collisionless, motivating a collisional gyrokinetic investigation. With the collision model introduced here, `stella` is well equipped for such problems.

Data availability statement

The data cannot be made publicly available upon publication because the cost of preparing, depositing and hosting the data would be prohibitive within the terms of this research project. The data that support the findings of this study are available upon reasonable request from the authors.

Acknowledgments

This work was supported by the Engineering and Physical Sciences Research Council (EPSRC) [EP/R034737/1].

Appendix A. Convergence of the Hirshman–Sigmar expansion

Using the definition of the Δ_j^{ab} and the orthogonality relation

$$\int v^l L_{j-1}^{\left(l+\frac{1}{2}\right)}\left(x_a^2\right)\Delta_j^{ab}\, v^2 \mathrm{d}v = 0 \tag{104}$$

it is straightforward to show by induction that for all $j < N$

$$\int v^l L_j^{\left(l+\frac{1}{2}\right)}\left(x_a^2\right)\Delta_N^{ab}\left[x_b^l L_N^{\left(l+\frac{1}{2}\right)} F_{0b}\right] v^2 \mathrm{d}v = 0. \tag{105}$$

Writing out the recursive expression for the Δ_j^{ab} (30) after $j+1-k$ steps one obtains

$$\Delta_{j+1}^{ab}[f] = \Delta_k^{ab}[f] - \sum_{i=k}^{j} \psi_i^{ab}[f]\,\Delta_i^{ab,l}, \tag{106}$$

where the $\Delta_j^{ab,l}$ are defined for compactness as given by (41). Then, for $k < j$

$$\Delta_j^{ab}\left[x_b^l L_k^{l+\frac{1}{2}} F_{0b}\right] = \Delta_k^{ab}\left[x_b^l L_k^{l+\frac{1}{2}} F_{0b}\right] \tag{107}$$

$$-\sum_{i=k}^{j-1} \frac{\int v^l L_k^{l+\frac{1}{2}}\Delta_i^{ab}\left[x_b^l L_i^{l+\frac{1}{2}} F_{0b}\right] v^2 dv}{\int v^l L_i^{l+\frac{1}{2}}\Delta_i^{ab}\left[x_b^l L_i^{l+\frac{1}{2}} F_{0b}\right] v^2 dv}\Delta_i^{ab,l}\left[x_b^l L_i^{l+\frac{1}{2}} F_{0b}\right]$$

$$= -\sum_{i=k+1}^{j-1} \frac{\int v^l L_k^{l+\frac{1}{2}}\Delta_i^{ab}\left[x_b^l L_i^{l+\frac{1}{2}} F_{0b}\right] v^2 dv}{\int v^l L_i^{l+\frac{1}{2}}\Delta_i^{ab}\left[x_b^l L_i^{l+\frac{1}{2}} F_{0b}\right] v^2 dv}\Delta_i^{ab,l}\left[x_b^l L_i^{l+\frac{1}{2}} F_{0b}\right]. \tag{108}$$

Invoking the orthogonality (105) yields

$$\Delta_j^{ab}\left[x_b^l L_k^{l+\frac{1}{2}} F_{0b}\right] = 0 \quad \text{for } k < j. \tag{109}$$

Taking $k = 0$ in (106) and rearranging, the exact isotropic component of the field particle operator can be written as

$$\begin{aligned} C_v^{ab}[f] := \Delta_0^{ab}[f] &= \sum_{j=0}^{N} \psi_j^{ab,l}[f]\,\Delta_j^{ab,l} + \Delta_{N+1}^{ab}[f] \\ &= C_v^{ab,N}[f] + \Delta_{N+1}^{ab}[f]. \end{aligned} \tag{110}$$

It follows immediately with (109) that the truncated operator $C_v^{ab,N}$ thus defined is exact for distribution functions of the form [13]

$$f_b^{(l)}(v) = \sum_{j=0}^{N} \frac{2}{v_{th,b}^{2l}} F_j^{(l)} v^l L_j^{(k)}\left(x_b^2\right) F_{0b}\left(x_b^2\right). \tag{111}$$

Since in the limit $N \to \infty$ any distribution function can be written in this way the approximate operator $C_v^{ab,N}(f)$ indeed converges to the exact field particle operator for $N \to \infty$ [13].

Appendix B. Calculation of C_v^l

The full field particle operator for collisions of f_b with F_{0a} is given by [see 12]

$$\begin{aligned} C[f_{a_0}, \delta f_b] = L^{ab} F_{0a} \Bigg[&\frac{m_a}{m_b}\delta f_b(v) + 2\frac{v}{v_\alpha^2}\left(1 - \frac{m_a}{m_b}\right)\frac{\partial \phi_{b_1}}{\partial v} \\ &+ \frac{2}{v_\alpha^2}\phi_{b_1}(v) - \left(\frac{2v}{v_\alpha^2}\right)^2 \frac{\partial^2 \psi_{b_1}}{\partial v^2}\Bigg]. \end{aligned} \tag{112}$$

We expand the Rosenbluth potentials in spherical harmonics, by using the generating function of the Legendre polynomials, P_l

$$\begin{aligned} \frac{1}{|\vec{v} - \vec{v}'|} &= \frac{1}{v\sqrt{1 + v'^2/v^2 - 2v'/v\cos\gamma}} \\ &= \frac{1}{v}\sum_{l=0}^{\infty}\left(\frac{v'}{v}\right)^l P_l(\cos\gamma), \end{aligned} \tag{113}$$

where $v' < v$ is required for convergence of the Legendre series, and γ denotes the angle between $\vec{v}$ and $\vec{v}'$. Using the addition theorem for the spherical harmonics it follows that

$$\frac{1}{|\vec{v} - \vec{v}'|} = \sum_{l=0}^{\infty}\sum_{m=-l}^{+l} \frac{4\pi}{2l+1}(-1)^m \frac{v_<^l}{v_>^{l+1}} Y_l^{-m}(\theta,\varphi)\, Y_l^m(\theta',\varphi'), \tag{114}$$

with $v_< := \min(v, v')$ and $v_> := \max(v, v')$. The first Rosenbluth potential is then given by

$$\begin{aligned} \phi_b(\vec{v}) = -\frac{1}{4\pi}\sum_{l=0}^{\infty}\sum_{m=-l}^{+l} \frac{4\pi}{2l+1}(-1)^m \Bigg[&Y_l^{-m}(\theta,\varphi) \\ &\times \iint Y_l^m(\theta',\varphi')\left(\frac{1}{v^{l+1}}\int_0^v v'^{l+2} f_b(\vec{v}')\,\mathrm{d}v' \right. \\ &\left. + v^l \int_v^\infty \frac{1}{v'^{l-1}} f_b(\vec{v}')\,\mathrm{d}v'\right)\mathrm{d}\Omega'\Bigg]. \end{aligned} \tag{115}$$

Using the orthogonality of the spherical harmonics it follows that for $f_b(\vec{v}) = f^{lm}(v) Y_l^m(\theta,\varphi)$

$$\begin{aligned} \phi_b(\vec{v}) = -\frac{1}{4\pi}\frac{4\pi}{2l+1} Y_l^m(\theta,\varphi)\Bigg(&\frac{1}{v^{l+1}}\int_0^v v'^{l+2} f^{lm}(v')\,\mathrm{d}v' \\ &+ v^l \int_v^\infty \frac{f^{lm}(v')}{v'^{l-1}}\,\mathrm{d}v'\Bigg). \end{aligned} \tag{116}$$

It follows that

$$\begin{aligned} \frac{\partial \phi_b(\vec{v})}{\partial v} = -\frac{1}{4\pi}\frac{4\pi}{2l+1} &Y_l^m(\theta,\varphi) \\ &\times \left(-\frac{l+1}{v^{l+2}}\int_0^v v'^{l+2} f^{lm}(v')\,\mathrm{d}v'\right. \qquad (117) \\ &\left. + l v^{l-1}\int_v^\infty \frac{f^{lm}(v')}{v'^{l-1}}\,\mathrm{d}v'\right). \qquad (118) \end{aligned}$$

To expand the second Rosenbluth potential, we multiply equation (113) by $(1 + v'^2/v^2 - 2v'/v\cos\gamma)$ and use the recurrence relation for the Legendre polynomials, $(2l+1)xP_l(x) = (l+1)P_{l+1}(x) + lP_{l-1}(x)$, to obtain, after some algebra and shifting of the summation indices

$$|\vec{v} - \vec{v}'| = \sum_{l=0}^{\infty} \frac{v_<^l}{v_>^{l+1}}\left[\frac{v_<^2}{2l+3} - \frac{v_>^2}{2l-1}\right] P_l(\cos\gamma). \tag{119}$$

It follows that

$$\begin{aligned} \psi_b(\vec{v}) = -\frac{1}{8\pi}\sum_{l=0}^{\infty}\sum_{m=-l}^{+l} \frac{4\pi}{2l+1}(-1)^m Y_l^{-m}(\theta,\varphi) \qquad (120) \\ \times \iint Y_l^m(\theta',\varphi')\left(\frac{1}{v^{l+1}}\int_0^v v'^{l+2}\right. \\ \times \left[\frac{v'^2}{2l+3} - \frac{v^2}{2l-1}\right] f_b(\vec{v}')\,\mathrm{d}v' \\ \left. + v^l \int_v^\infty \frac{1}{v'^{l-1}}\left[\frac{v^2}{2l+3} - \frac{v'^2}{2l-1}\right] f_b(\vec{v}')\,\mathrm{d}v'\right)\mathrm{d}\Omega. \qquad (121) \end{aligned}$$

Then, for a distribution function of the form $f_b(\vec{v}) = f^{lm}(v)Y_l^m(\theta,\varphi)$

$$\frac{\partial^2\psi_b(\vec{v})}{\partial v^2} = -\frac{1}{8\pi}\frac{4\pi}{2l+1}Y_l^m(\theta,\varphi)\left[\frac{(l+1)(l+2)}{2l+3}\right.$$
$$\times\left(\frac{1}{v^{l+3}}\int_0^v v'^{l+4}f^{lm}(v')\,\mathrm{d}v' + v^l\int_v^\infty\frac{f^{lm}(v')}{v'^{l-1}}\,\mathrm{d}v'\right)$$
$$-\frac{l(l-1)}{2l-1}\left(\frac{1}{v^{l+1}}\int_0^v v'^{l+2}f^{lm}(v')\,\mathrm{d}v'\right.$$
$$\left.\left.+v^{l-2}\int_v^\infty\frac{f^{lm}(v')}{v'^{l-3}}\,\mathrm{d}v'\right)\right], \tag{122}$$

whence the field particle operator is given by

$$\begin{aligned}
&C[F_{0a},f_b^{(lm)}(v)Y_l^m(\theta,\varphi)]\\
&= L^{ab}F_{0a}Y_l^m(\theta,\varphi)\frac{1}{2l+1}\left[(2l+1)\mu_{ab}f_b^{(lm)}(v)\right.\\
&\quad-2\frac{v}{v_\alpha^2}(1-\mu_{ab})\times\left(-\frac{l+1}{v^{l+2}}\int_0^v v'^{l+2}f_b^{(lm)}(v')\,\mathrm{d}v'\right.\\
&\quad\left.+lv^{l-1}\int_v^\infty\frac{f_b^{(lm)}(v')}{v'^{l-1}}\,\mathrm{d}v'\right)\\
&\quad-\frac{2}{v_\alpha^2}\left(\frac{1}{v^{l+1}}\int_0^v v'^{l+2}f_b^{(lm)}(v')\,\mathrm{d}v' + v^l\int_v^\infty\frac{f_b^{(lm)}(v')}{v'^{l-1}}\,\mathrm{d}v'\right)\\
&\quad+\frac{1}{2}\left(\frac{2v}{v_\alpha^2}\right)^2\left\{\frac{(l+1)(l+2)}{2l+3}\left(\frac{1}{v^{l+3}}\int_0^v v'^{l+4}f_b^{(lm)}(v')\,\mathrm{d}v'\right.\right.\\
&\quad\left.+v^l\int_v^\infty\frac{f_b^{(lm)}(v')}{v'^{l-1}}\,\mathrm{d}v'\right)\\
&\quad-\frac{l(l-1)}{2l-1}\left(\frac{1}{v^{l+1}}\int_0^v v'^{l+2}f_b^{(lm)}(v')\,\mathrm{d}v'\right.\\
&\quad\left.\left.\left.+v^{l-2}\int_v^\infty\frac{f_b^{(lm)}(v')}{v'^{l-3}}\,\mathrm{d}v'\right)\right\}\right]\\
&= Y_l^m(\theta,\varphi)C_v^{(l)}[f_b^{(lm)}(v)].
\end{aligned}\tag{123}$$

The spherical harmonics are therefore eigenfunctions of the field particle collision operator. The calculation of the basis functions $\Delta_j^{l+\frac{1}{2},ab}\left[x_b^lL_j^{(l+1/2)}(x_b^2)\exp(-x_b^2)\right]$ for the Hirshman-Sigmar expansion of the field particle operator requires the calculation of

$$\Delta_0^{l+\frac{1}{2},ab}\left[x_b^lL_j^{(l+1/2)}\left(x_b^2\right)\exp\left(-x_b^2\right)\right] = C_v^{ab}\left[F_{0a},x_b^lL_j^{(l+1/2)}\left(x_b^2\right)\exp\left(-x_b^2\right)\right]. \tag{124}$$

The resulting integral expressions over Laguerre polynomials can be simplified by using the definition of the generalised Laguerre polynomials

$$L_j^{\left(l+\frac{1}{2}\right)}(x) = \sum_{k=0}^j\underbrace{\frac{(-1)^k(l+j+1/2)!}{(j-k)!(l+k+1/2)!k!}}_{=:c_k^{jl}}x^k \tag{125}$$

After some algebra and introducing the lower and upper incomplete Gamma functions, $\gamma(s,x)$ and $\Gamma(s,x)$, respectively [see 11], one obtains

$$\begin{aligned}
&\Delta_0^{l+\frac{1}{2},ab}\left[x_b^lL_j^{(l+1/2)}(x_b^2)\exp(-x_b^2)\right]\\
&= L^{ab}\mu_{ab}\exp(-x_a^2)\frac{1}{2l+1}\sum_{i=0}^j c_i^{jl}\left[(2l+1)x_b^{l+2i}\exp(-x_b^2)\right.\\
&\quad-x_b(1-\mu_{ab})\left(-\frac{l+1}{x_b^{l+2}}\gamma(3/2+l+i,x_b^2)\right.\\
&\quad\left.+lx_b^{l-1}\Gamma(1+i,x_b^2)\right)\\
&\quad-\left(\frac{1}{x_b^{l+1}}\gamma(3/2+l+i,x_b^2)+x_b^l\Gamma(1+i,x_b^2)\right)\\
&\quad+\mu_{ab}x_b^2\frac{(l+1)(l+2)}{2l+3}\left(\frac{1}{x_b^{l+3}}\gamma(5/2+l+i,x_b^2)\right.\\
&\quad\left.+x_b^l\Gamma(1+i,x_b^2)\right)\\
&\quad-\mu_{ab}x_b^2\frac{l(l-1)}{2l-1}\left(\frac{1}{x_b^{l+1}}\gamma(3/2+l+i,x_b^2)\right.\\
&\quad\left.\left.+x_b^{l-2}\Gamma(2+i,x_b^2)\right)\right].
\end{aligned}\tag{126}$$

Appendix C. Fourier components of the gyroaveraged test-particle operator

We calculate the Fourier components of the gyroaveraged test-particle operator expressed in $(v_\parallel,\mu)$-coordinates. Since the gyro-average is taken at fixed guiding center $\boldsymbol{R}$, the velocity derivatives in the collision operator are first transformed to derivatives at fixed $\boldsymbol{R}$

$$\begin{aligned}
\left.\frac{\partial}{\partial\varphi}\right|_{\boldsymbol{r}} &= \left.\frac{\partial}{\partial\varphi}\right|_{\boldsymbol{R}} + \frac{\partial\boldsymbol{R}}{\partial\varphi}\left.\frac{\partial}{\partial\boldsymbol{R}}\right|_{\boldsymbol{v}} = \left.\frac{\partial}{\partial\varphi}\right|_{\boldsymbol{R}} - \frac{1}{\Omega}\frac{\partial}{\partial\varphi}\left(\hat{\boldsymbol{b}}\times\boldsymbol{v}_\perp\right)\left.\frac{\partial}{\partial\boldsymbol{R}}\right|_{\boldsymbol{v}}\\
&= \left.\frac{\partial}{\partial\varphi}\right|_{\boldsymbol{R}} + \frac{\boldsymbol{v}_\perp}{\Omega}\cdot\left.\frac{\partial}{\partial\boldsymbol{R}}\right|_{\boldsymbol{v}}
\end{aligned}\tag{127}$$

$$\begin{aligned}
\left.\frac{\partial}{\partial\mu}\right|_{\boldsymbol{r}} &= \left.\frac{\partial}{\partial\mu}\right|_{\boldsymbol{R}} + \frac{\partial\boldsymbol{R}}{\partial\mu}\left.\frac{\partial}{\partial\boldsymbol{R}}\right|_{\boldsymbol{v}} = \left.\frac{\partial}{\partial\mu}\right|_{\boldsymbol{R}} - \frac{\hat{\boldsymbol{b}}}{\Omega}\times\frac{\partial\boldsymbol{v}_\perp}{\partial\mu}\left.\frac{\partial}{\partial\boldsymbol{R}}\right|_{\boldsymbol{v}}\\
&= \left.\frac{\partial}{\partial\mu}\right|_{\boldsymbol{R}} - \frac{1}{2\mu}\boldsymbol{\rho}\cdot\left.\frac{\partial}{\partial\boldsymbol{R}}\right|_{\boldsymbol{v}}
\end{aligned}\tag{128}$$

$$\left.\frac{\partial}{\partial v_\parallel}\right|_{\boldsymbol{r}} = \left.\frac{\partial}{\partial v_\parallel}\right|_{\boldsymbol{R}} + \frac{\partial\boldsymbol{R}}{\partial v_\parallel}\left.\frac{\partial}{\partial\boldsymbol{R}}\right|_{\boldsymbol{v}} = \left.\frac{\partial}{\partial v_\parallel}\right|_{\boldsymbol{R}} \tag{129}$$

where we used that $\mu = mv_\perp^2/2B_0$, so that $\partial_\mu\boldsymbol{v}_\perp = \boldsymbol{v}_\perp/v_\perp^2\cdot B_0/m = \boldsymbol{v}_\perp/\mu/2$. We now perform the gyro-averaging operation (45). The $v_\parallel$-component of the collision operator is unaffected. Aligning $\boldsymbol{k}$ with the $\varphi = 0$ axis

$$\begin{aligned}
&\frac{\partial}{\partial\mu}\left(e^{-i\boldsymbol{k}\cdot\boldsymbol{\rho}}h_{\boldsymbol{k}}/F_0\right)\\
&\quad=\frac{\partial}{\partial\mu}\left(e^{-i\boldsymbol{k}\cdot(\hat{\boldsymbol{b}}\times\boldsymbol{v}_\perp)/\Omega}h_{\boldsymbol{k}}/F_0\right)\\
&\quad=\frac{\partial}{\partial\mu}\left(e^{ikv_\perp\sin\varphi/\Omega}h_{\boldsymbol{k}}/F_0\right)\\
&\quad=\frac{\partial}{\partial\mu}\left(e^{ik\sqrt{2B_0\mu/m}\sin\varphi/\Omega}h_{\boldsymbol{k}}/F_0\right)\\
&\quad=ik\frac{B_0\sin\varphi}{mv_\perp\Omega}e^{ikv_\perp\sin\varphi/\Omega}h_{\boldsymbol{k}}/F_0+e^{ikv_\perp\sin\varphi/\Omega}\frac{\partial}{\partial\mu}\left(h_{\boldsymbol{k}}/F_0\right).
\end{aligned}\tag{130}$$

The gyroaverage of the μ-component of the collision operator then yields

$$\begin{aligned}
&\left\langle e^{i\boldsymbol{k}\cdot\boldsymbol{\rho}}\frac{\partial}{\partial\mu}\left(\gamma_\mu F_0\left[ik\frac{B_0\sin\varphi}{mv_\perp\Omega}e^{-i\boldsymbol{k}\cdot\boldsymbol{\rho}}\frac{h_{\boldsymbol{k}}}{F_0}+e^{-i\boldsymbol{k}\cdot\boldsymbol{\rho}}\frac{\partial}{\partial\mu}\frac{h_{\boldsymbol{k}}}{F_0}\right]\right)\right\rangle\\
&\qquad=\frac{\partial}{\partial\mu}\left(\gamma_\mu F_0\frac{\partial}{\partial\mu}\frac{h_{\boldsymbol{k}}}{F_0}\right)-\frac{k^2}{4\Omega^2}\left[\nu_\parallel v_\perp^2+\nu_D v_\parallel^2\right]h_{\boldsymbol{k}}
\end{aligned}\tag{131}$$

where we used that $\langle\sin\varphi\rangle=\langle\cos\varphi\rangle=\langle\cos\varphi\sin\varphi\rangle=0$. The mixed-differential components of the operator are unchanged because the gyro-average over $\boldsymbol{\rho}$ vanishes. For the φ-differential component of the operator

$$\begin{aligned}
&\left\langle e^{i\boldsymbol{\rho}\cdot\boldsymbol{k}}\frac{\nu_D}{2}\left(1+\frac{mv_\parallel^2}{2B_0\mu}\right)\frac{\partial^2 e^{-i\boldsymbol{\rho}\cdot\boldsymbol{k}}h_{\boldsymbol{k}}}{\partial\varphi^2}\right\rangle\\
&\qquad=\left\langle-\frac{\nu_D}{2}\left(1+\frac{mv_\parallel^2}{2B_0\mu}\right)\frac{k^2v_\perp^2\cos^2\varphi}{\Omega^2}\right\rangle\\
&\qquad=-\nu_D\frac{k^2v^2}{4\Omega^2}h_{\boldsymbol{k}}.
\end{aligned}\tag{132}$$

Collecting the μ-, $v_\parallel$- and φ-terms, the gyrokinetic test-particle collision operator in Fourier space is given by

$$\begin{aligned}
C_{\mathrm{GK,test}}[h_{\boldsymbol{k}_\perp}]=&\frac{\partial}{\partial v_\parallel}\left[\gamma_{v_\parallel}^{ab}F_0\frac{\partial}{\partial v_\parallel}\frac{h_{\boldsymbol{k}_\perp}}{F_0}+v_\parallel\mu\nu_x^{ab}F_0\frac{\partial}{\partial\mu}\frac{h_{\boldsymbol{k}_\perp}}{F_0}\right]\\
&+\frac{\partial}{\partial\mu}\left[\gamma_\mu^{ab}F_0\frac{\partial}{\partial\mu}\frac{h_{\boldsymbol{k}_\perp}}{F_0}+v_\parallel\mu\nu_x^{ab}F_0\frac{\partial}{\partial v_\parallel}\frac{h_{\boldsymbol{k}_\perp}}{F_0}\right]\\
&-\frac{1}{2}\left(\nu_\parallel\frac{B_0\mu}{m}+\nu_D\left[v_\parallel^2+\frac{B_0\mu}{m}\right]\right)\frac{k^2\rho^2}{v_{th}^2}h_{\boldsymbol{k}_\perp},
\end{aligned}\tag{133}$$

where we have used that $\rho=v_{th}/\Omega$.

ORCID iDs

A von Boetticher https://orcid.org/0009-0009-6559-9433
M Barnes https://orcid.org/0000-0002-0177-1689

References

[1] Abel I G, Barnes M, Cowley S C, Dorland W and Schekochihin A A 2008 Linearized model Fokker-Planck collision operators for gyrokinetic simulations. I. Theory *Phys. Plasmas* **15** 122509
[2] Alcusón J A, Xanthopoulos P, Plunk G G, Helander P, Wilms F, Turkin Y, von Stechow A and Grulke O 2020 Suppression of electrostatic micro-instabilities in maximum-j stellarators *Plasma Phys. Control. Fusion* **62** 035005
[3] Anderson E *et al* 1999 *Lapack Users' Guide* 3rd edn (Society for Industrial and Applied Mathematics)
[4] Barnes M, Abel I G, Dorland W, Ernst D R, Hammett G W, Ricci P, Rogers B N, Schekochihin A A and Tatsuno T 2009 Linearized model Fokker-Planck collision operators for gyrokinetic simulations. II. Numerical implementation and tests *Phys. Plasmas* **16** 072107
[5] Barnes M, Parra-Diaz F and Landreman M 2018 `stella`: a mixed implicit-explicit, delta-f gyrokinetic code for general magnetic field configurations (arXiv:1806.02162)
[6] Belli E A and Candy J 2008 Kinetic calculation of neoclassical transport including self-consistent electron and impurity dynamics *Plasma Phys. Control. Fusion* **50** 095010
[7] Belli E A and Candy J 2011 Full linearized fokker–planck collisions in neoclassical transport simulations *Plasma Phys. Control. Fusion* **54** 015015
[8] Dimits A M *et al* 2000 Comparisons and physics basis of tokamak transport models and turbulence simulations *Phys. Plasmas* **7** 969–83
[9] García-Regaña J M *et al* 2020 Turbulent impurity transport simulations in Wendelstein 7-X plasmas *J. Plasma Phys.* **87**
[10] Geiger B *et al* 2019 Observation of anomalous impurity transport during low-density experiments in W7-X with laser blow-off injections of iron *Nucl. Fusion* **59** 046009
[11] Gradshteyn I S and Ryzhik I M 2007 *Table of Integrals, Series and Products* 7th edn (Elsevier/Academic)
[12] Helander P and Sigmar D J 2002 *Collisional Transport in Magnetized Plasmas* (*Cambridge Monographs on Plasma Physics*)(Cambridge University Press)
[13] Hirshman S P and Sigmar D J 1976 Approximate fokker–planck collision operator for transport theory applications *Phys. Fluids* **19** 1532–40
[14] Howes G G, Cowley S C, Dorland W, Hammett G W, Quataert E and Schekochihin A A 2006 Astrophysical gyrokinetics: basic equations and linear theory *Astrophys. J.* **651** 590–614
[15] Kauffmann K, Kleiber R, Hatzky R and Borchardt M 2010 Global linear gyrokinetic simulations for LHD including collisions *J. Phys.: Conf. Ser.* **260** 012014
[16] Klinger T *et al* 2019 Overview of first Wendelstein 7-X high-performance operation *Nucl. Fusion* **59** 112004
[17] Kotschenreuther M, Rewoldt G and Tang W 1995 Comparison of initial value and eigenvalue codes for kinetic toroidal plasma instabilities *Comput. Phys. Commun.* **88** 128–40
[18] Kálnay de Rivas E 1972 On the use of nonuniform grids in finite-difference equations *J. Comput. Phys.* **10** 202–10
[19] Landau L 1936 The transport equation in the case of Coulomb interactions *Phys. Z. Sowjet* **10** 154
[20] Langenberg A *et al* 2018 Impurity transport studies at Wendelstein 7-X by means of x-ray imaging spectrometer measurements *Plasma Phys. Control. Fusion* **61** 014030

[21] Onsager L 1931 Reciprocal relations in irreversible processes. I *Phys. Rev.* **37** 405–26
[22] Pan Q, Ernst D R and Crandall P 2020 First implementation of gyrokinetic exact linearized landau collision operator and comparison with models *Phys. Plasmas* **27** 042307
[23] Pan Q, Ernst D R and Hatch D R 2021 Importance of gyrokinetic exact Fokker-Planck collisions in fusion plasma turbulence *Phys. Rev.* E **103** L051202
[24] Sánchez E, Estrada T, Velasco J, Calvo I, Cappa A, Alonso A, García-Regaña J, Kleiber R and and J R 2019 Validation of global gyrokinetic simulations in stellarator configurations *Nucl. Fusion* **59** 076029
[25] Sugama H, Watanabe T-H and Nunami M 2009 Linearized model collision operators for multiple ion species plasmas and gyrokinetic entropy balance equations *Phys. Plasmas* **16** 112503